MOLECULAR METABOLISM

Loss of carnitine palmitoyltransferase 1a reduces docosahexaenoic acid-containing phospholipids and drives sexually dimorphic liver disease in mice

Mikala M. Zelows [1], Corissa Cady [2], Nikitha Dharanipragada [3], Anna E. Mead [3], Zachary A. Kipp [3], Evelyn A. Bates [3], Venkateshwari Varadharajan [4], Rakhee Banerjee [4], Se-Hyung Park [3,5], Nathan R. Shelman [6], Harrison A. Clarke [7,8], Tara R. Hawkinson [7,8], Terrymar Medina [7,8], Ramon C. Sun [7,8], Todd A. Lydic [9], Terry D. Hinds Jr. [3,10,11], J. Mark Brown [4], Samir Softic [3,5], Gregory A. Graf [2,12], Robert N. Helsley [3,10,11,12,13,*]

ABSTRACT

Background and aims: Genome and epigenome wide association studies identified variants in carnitine palmitoyltransferase 1a (CPT1a) that associate with lipid traits. The goal of this study was to determine the role of liver-specific CPT1a on hepatic lipid metabolism.

Approach and results: Male and female liver-specific knockout (LKO) and littermate controls were placed on a low-fat or high-fat diet (60% kcal fat) for 15 weeks. Mice were necropsied after a 16 h fast, and tissues were collected for lipidomics, matrix-assisted laser desorption ionization mass spectrometry imaging, kinome analysis, RNA-sequencing, and protein expression by immunoblotting. Female LKO mice had increased serum alanine aminotransferase levels which were associated with greater deposition of hepatic lipids, while male mice were not affected by CPT1a deletion relative to male control mice. Mice with CPT1a deletion had reductions in DHA-containing phospholipids at the expense of monounsaturated fatty acids (MUFA)-containing phospholipids in whole liver and at the level of the lipid droplet (LD). Male and female LKO mice increased RNA levels of genes involved in LD lipolysis (*Plin2*, *Cidec*, *G0S2*) and in polyunsaturated fatty acid metabolism (*Elovl5*, *Fads1*, *Elovl2*), while only female LKO mice increased genes involved in inflammation (*Ly6d*, *Mmp12*, *Cxcl2*). Kinase profiling showed decreased protein kinase A activity, which coincided with increased PLIN2, PLIN5, and G0S2 protein levels and decreased triglyceride hydrolysis in LKO mice.

Conclusions: Liver-specific deletion of CPT1a promotes sexually dimorphic steatotic liver disease (SLD) in mice, and here we have identified new mechanisms by which females are protected from HFD-induced liver injury.

Keywords Triglycerides; Lipid droplets; Mitochondria; Lipolysis; Fatty acid metabolism

1. INTRODUCTION

Steatotic liver disease (SLD) is a spectrum of disease etiologies ranging from simple steatosis to metabolic dysfunction-associated steatohepatitis (MASH) [1,2]. Over 64 million people in the United States are projected to have SLD, which is associated with a decrease in lifespan [3] and is expected to become the leading cause of liver-related morbidity and mortality over the next 15 years [4]. Intriguingly, SLD is largely considered a sexually dimorphic disease with a greater prevalence in men [5], but women exhibit a greater risk of progressing to more severe SLD [6]. Evidence from rodent and human studies has shown that pre-menopausal women are protected from SLD, in part, due to their ability to partition fatty acids towards oxidation and away from the secretory pathway [7,8]. While it is widely appreciated that

[1]Department of Pharmaceutical Sciences, University of Kentucky College of Pharmacy, Lexington, KY, USA [2]Department of Physiology, University of Kentucky College of Medicine, Lexington, KY, USA [3]Department of Pharmacology and Nutritional Sciences, University of Kentucky College of Medicine, Lexington, KY, USA [4]Department of Cancer Biology, Lerner Research Institute, Cleveland Clinic, Cleveland, OH, USA [5]Department of Pediatrics and Gastroenterology, University of Kentucky College of Medicine, Lexington, KY, USA [6]Department of Pathology and Laboratory Medicine, University of Kentucky College of Medicine, Lexington, KY, USA [7]Department of Biochemistry & Molecular Biology, University of Florida College of Medicine, Gainesville, FL, USA [8]Center for Advanced Spatial Biomolecule Research, University of Florida College of Medicine, Gainesville, FL, USA [9]Department of Physiology, Michigan State University, East Lansing, MI, USA [10]Barnstable Brown Diabetes Center, University of Kentucky College of Medicine, Lexington, KY, USA [11]Markey Cancer Center, University of Kentucky College of Medicine, Lexington, KY, USA [12]Saha Cardiovascular Research Center, University of Kentucky, Lexington, KY, USA [13]Department of Internal Medicine, Division of Endocrinology, Diabetes, and Metabolism, University of Kentucky College of Medicine, Lexington, KY, USA

*Corresponding author. 741 S. Limestone St., BBSRB B347 Lexington, KY 40536, USA. Tel.: +859 218 1608. E-mail: robert.helsley@uky.edu (R.N. Helsley).

Abbreviations: CPT1a, Carnitine Palmitoyltransferase 1a; SLD, Steatotic Liver Disease; PKA, Protein Kinase A; LD, Lipid droplet; DHA, Docosahexaenoic acid; MUFA, Monounsaturated fatty acid; PUFA, Polyunsaturated fatty acid; MALDI-MSI, Matrix-assisted laser desorption ionization for mass spectrometry imaging; FAO, Fatty acid oxidation; ALT, Alanine aminotransferase; HFD, High fat diet; LFD, Low fat diet; PPAR, Peroxisome proliferator-activated receptor

1

estrogen elicits anti-inflammatory and pro-fatty acid oxidation (FAO) properties [9], less is known about downstream signaling pathways that elicit protection from SLD.

The carnitine palmitoyltransferase 1 (CPT1) gene family consists of three isoforms (1a, 1b, 1c) that differ in subcellular localization, tissue specificity, and function [10]. The CPT1a and CPT1b isoforms are considered to be primarily expressed in the liver and muscle, respectively, where they reside on the outer mitochondrial membrane to convert long-chain acyl-CoAs to acylcarnitines for entry into the mitochondria and subsequent fatty acid oxidation (FAO) [10]. Genome- and epigenome-wide associations studies have identified loss-of-function variants in CPT1a that associate with lower triglycerides [11—13], ω3-polyunsaturated fatty acids (PUFAs) including docosa-hexaenoic acid (DHA), and increased circulating monounsaturated fatty acids (MUFAs) [14]. However, little is known about the mechanisms explaining these associations.

We characterized the contribution of hepatic CPT1a to hepatic lipid metabolic phenotypes in male and female mice. Using a CPT1a liver-specific deficient mouse model, we show female mice depend on CPT1a for protection from the high-fat diet (HFD)-induced liver dysfunction. Male mice are more susceptible to HFD-induced liver dysfunction than female control mice, a condition that is not worsened by the absence of CPT1a. Utilizing a combination of lipidomic approaches, we demonstrate that hepatic CPT1a-deficiency alters the total phospholipid pool and promotes the incorporation of mono-unsaturated (MUFA)-containing phospholipids at the expense of do-cosahexaenoic acid (DHA)-containing phospholipids in lipid droplets (LD). The shift in MUFA from DHA-containing phospholipids within LDs associates with increases in PUFA-biosynthetic and peroxisome pro-liferator activated receptor (PPAR)-target gene expression. Mechanis-tically, kinase profiling of liver samples shows reductions in protein kinase A (PKA) activity, which coincided with impaired triglyceride hydrolysis in CPT1a-deficient livers. These studies reveal new mech-anisms by which impairments in long-chain fatty acid oxidation drive sexually dimorphic SLD and alter LD dynamics in mice.

2. EXPERIMENTAL PROCEDURES

2.1. Experimental design and study subjects

Animal protocols were in accordance with NIH guidelines and approved by the Institutional Animal Care and Use Committee at the University of Kentucky. Mice were housed in individually ventilated cages at 20—22 °C on a 14 h light/10 h dark cycle with ad libitum access to food and water. CPT1a-floxed mice were obtained from the laboratory of Dr. Peter Carmeliet [15], backcrossed >10 generations on the C57BL/6 back-ground, and then were bred with the Albumin-Cre (Jackson Laboratory) transgenic mice to achieve liver-specific knockdown of CPT1a. Six to 8-week-old littermate controls (floxed & LKO) were fed either a semi-purified low-fat diet (10% kcal from fat; Research Diets, D12450K) or a high-fat diet (60% kcal from fat; Research Diets, D12492) for 15-weeks prior to necropsy. Mice were necropsied after a 16-hour (4 PM—8 AM) fast to induce adipose tissue lipolysis and concomitant hepatic FAO. Indirect calorimetry was completed on mice after 7 weeks of HFD feeding using the Promethion metabolic cages (Sable Systems Inter-national). Magnetic resonance relaxometry (Echo-MRI-100TM, Echo Medical System, Houston, TX) was used to assess total body fat, lean mass, and fat mass in mice at baseline, 7, and 15 weeks on the diet. For intraperitoneal glucose tolerance tests, mice were fasted overnight and were injected into the peritoneal cavity with a 20% glucose so-lution at a volume of 10 μL per gram of body weight. For insulin

tolerance tests, baseline glucose levels were measured in the fed state (at 8 AM), then mice were then injected into the peritoneal cavity with 1 U/kg of insulin. Serum glucose levels were measured using the IN-FINITY glucometer and glucose strips (ADW). Serum insulin (Crystal Chem) and β-hydroxybutyrate (Cayman Chem) levels were quantified using commercial assays according to manufacturers' instructions.

2.2. Quantification of hepatic lipids

Extraction of liver lipids and subsequent quantification of hepatic tri-glycerides, total cholesterol, and phosphatidylcholine were conducted using enzymatic assays as previously described [16,17]. Liver samples were delipidated in 4 mL of 2:1 chloroform to methanol (v/v) overnight. The organic solvent was dried under a constant stream of N_2 prior to adding 6 mL of 2:1 chloroform to methanol. To separate the phases, 1.2 mL of 0.05% H_2SO_4 was added, samples were vortexed then centrifuged at 2000 rpm for 15 min. The bottom (organic) phase was recorded, and 0.5 mL of the organic phase was added to 1 mL of 1% TritonX-100 in chloroform. The samples were dried under N_2 and 0.5 mL H_2O was added prior to quantification of triglycerides (Wako), total cholesterol (Pointe Scientific), and choline-containing phospho-lipids (Sigma), per manufacturer's instructions. All standards and blanks were prepared in a similar fashion, and data were presented normalized to initial liver weights.

2.3. Histological analysis

Hematoxylin and eosin (H&E) staining of formalin-fixed paraffin-embedded liver sections was performed as previously described [16,17]. LD number and size were calculated by blinded members of the laboratory. In short, 2 individuals (independent of one another) captured 3 fields surrounding the portal vein and 3 fields surrounding the central vein at 100× magnification on a Nikon AR15. A total of 6 fields were captured per section, per mouse, for a total of 240 fields (e.g., 2 sections/per mouse for 20 total mice). The diameter was calculated for each individual droplet using Nikon Elements. The total number of LDs was normalized to the total nuclei in a given field.

2.4. Serum ALT levels

To determine the degree of liver injury in control and LKO mice, alanine aminotransferase (ALT) levels were measured in serum using enzy-matic assays (Sekisui Diagnostics, Lexington, MA, USA), as previously described [16,17].

2.5. Shotgun lipidomics

2.5.1. Lipid extraction

Liver samples on dry ice were spiked with 10 microliters of an internal standard and calibration mixture consisting of 500 μM each of di-myristoyl phospholipids (PG, PE, PS, PA, PC), 500 μM SM (30:1) and 50 μM TG (14:1/14:1/14:1). To each sample, 300 μL of −20 °C chilled 75% methanol containing 0.01% BHT (butylated hydroxytoluene) were added along with 0.5 mm zirconium oxide beads. Samples were ho-mogenized briefly in a Bullet Blender tissue homogenizer and placed on ice. Sixty microliters of methanol and 1 mL of MTBE were added to each sample, and samples were then vortexed for 60 min at room temperature. Water (170 μL) was added, and the samples were vor-texed for an additional 15 min and then centrifuged for 15 min. The supernatants were collected to new test tubes and precipitated pro-teins were re-extracted as above. Pooled extracts were dried overnight in a speedvac, and resuspended in 400 μL of isopropanol containing 0.01% BHT.

2.5.2. Lipidomics analysis by Orbitrap high resolution/accurate mass spectrometry

Immediately prior to analysis, aliquots of each lipid extract were diluted 50-fold in isopropanol: methanol (2:1, v:v) containing 20 mM ammonium formate. Full scan MS spectra at 100,000 resolution (defined at m/z 400) were collected on a Thermo Scientific LTQ-Orbitrap Velos mass spectrometer in both positive and negative ionization modes. Scans were collected from m/z 200 to m/z 1200. For each analysis, 10 μL of sample was directly introduced by flow injection [18,19] at 10 μL/min using an electrospray ionization source equipped with a fused silica ESI needle to minimize intrasource accumulation of triglycerides. A Shimadzu Prominence HPLC with thermostatted autosampler served as the sample delivery unit. The sample and injection solvent were 2:1 (v: v) isopropanol: methanol containing 20 mM ammonium formate. The spray voltage was 4.5 kV, ion transfer tube temperature was 275 °C, the S-lens value was 50 percent, and the Orbitrap fill time was 100 ms. The autosampler was set to 4 °C. After 2 min of MS signal averaging, the LC tubing, autosampler, and ESI source were flushed with 1 mL of isopropanol, prior to injection of the next sample. Samples were analyzed in random order, interspersed by solvent blank injections, extraction blank injections, and pooled QC samples derived from all study samples. Following MS data acquisition, offline mass recalibration was performed with the "Recalibrate Offline" tool in Thermo Xcalibur software according to the vendor's instructions, using the theoretical computed masses for the internal calibration standards and several common endogenous mammalian lipid species. MS/MS confirmation and structural analysis of lipid species identified by database searching were performed using higher-energy collisional dissociation (HCD) MS/MS at 60,000 resolution and a normalized collision energy of 25 for positive ion mode, and 60 for negative ion mode. MS/MS scans were triggered by inclusion lists generated separately for positive and negative ionization modes.

2.5.3. Lipid peak finding, identification, and quantitation

Lipids were identified using the Lipid Mass Spectrum Analysis (LIMSA) v.1.0 software linear fit algorithm, in conjunction with an in-house database of hypothetical lipid compounds, for automated peak finding and correction of ^{13}C isotope effects as previously described [20]. Peak areas of found peaks were quantified by normalization against an internal standard of a similar lipid class. The top ∼300 most abundant peaks in both positive and negative ionization mode were then selected for MS/MS inclusion lists and imported into Xcalibur software for structural analysis on the pooled QC sample as described above. For this untargeted analysis, no attempt was made to correct for differences in lipid species ionization due to the length or degree of unsaturation of the esterified fatty acids. Therefore, lipid abundance values are inherently estimates rather than true 'absolute' values, and so all data are presented as % of the total pool of lipid.

2.6. Spatial lipidomics

High-performance liquid chromatography (HPLC)-methanol, HPLC-grade water and N-(1-Naphthyl)ethylenediamine dihydrochloride (NEDC) matrix were obtained from Sigma-Aldrich. Slides were prepared similar as previously described [21]. After desiccation for one hour, slides were sprayed with 14 passes of 7 mg/mL NEDC matrix in 70% methanol, applied at 0.06 mL/min with a 3 mm offset and a velocity of 1200 mm/min at 30 °C and 10psi using the M5 Sprayer with a heated tray of 50 °C. Slides were used immediately or stored in a desiccator until use. For the detection of lipids, a Bruker timsTOF QTOF high-definition mass spectrometer was used. The laser was operating at 10000 Hz with 60% laser energy, with 300 laser shots per pixel and spot size of 50 μm at X and Y coordinates of 50 μm with mass range set at 50−2000 m/z in negative mode. Data acquisition spectrums were uploaded to Scils Software (Bruker Corporation) for the generation of small molecule and lipid images. Regions of interest (ROIs) were drawn around the whole tissue. For all pixels defined within a ROI, peak intensities were averaged and normalized by total ion current.

2.7. LD Isolation from Mouse Liver

Male and female control and LKO mice were fed a HFD for 15-weeks. After 15-weeks of feeding, mice were necropsied in the fasted state and LDs were isolated by sucrose gradient centrifugation as we have previously described [17]. LD PC and PE lipids were extracted and quantified using the targeted LC-MS/MS method below [17].

2.8. Relative Quantitation of Phosphatidylcholine (PC) and Phosphatidylethanolamine (PE) Lipid Species in LD Fractions

A targeted lipidomic assay for PC and PE lipids was developed using HPLC on-line electrospray ionization tandem mass spectrometry (LC/ESI/MS/MS), as previously described [17].

2.8.1. Standard Solutions and Lipid Extraction

The standards (PC_36:4 and PE_34:2) and the isotope labeled internal standards (PC_33:1-d7 and PE_31:1-d7) were purchased from Avanti Polar Lipids (Alabaster, Alabama, USA). The Standard solution at concentrations of 0, 10, 50, 200, 1000, 5000 and 20000 ng/ml were prepared in 80% methanol containing the internal standard at the concentration of 500 ng/ml. Tissue homogenate with a volume of 20 μl was mixed with 80 μl methanol containing 2 internal standards at the concentration of 625 ng/ml, vortexed for 30 sec and then centrifuged at 18000 rcf, 4 C for 12 min. After centrifugation, 50 ul supernatant was transferred into a HPLC vial for injection. The volume of 5 μl standard solution and extracted sample was injected into the Vanquish UHPLC system (Thermos Fisher Scientific, Waltham, MA, USA) for lipid separation.

2.8.2. LC/MS/MS Parameters

A C18 column (2.1 × 150 mm, Gemini, 3 μm, Phenomenex,) was used for the separation of the lipid species. Mobile phases were A (water containing 0.1% acetic acid and 0.3% ammonium hydroxide) and B (methanol/acetonitrile, 1/1 (v/v)) containing 0.1% acetic acid and 0.3% ammonium hydroxide). Mobile phase B at 80% was used from 0 to 2 min at the flow rate of 0.3 mL/min and then a linear gradient from 80% B to 100% B from 2 to 8 min, kept at 100% B from 8 to 20 min, 100% B to 80% B from 20 to 20.1 min, kept 80% B from 20.1 to 29 min. The HPLC eluent was directly injected into a triple quadrupole mass spectrometer (TSQ Quantiva, Thermos Fisher Scientific, Waltham, MA, USA) and both the PC and PE lipids were ionized at the positive mode. The PC species were monitored using Selected Reaction Monitoring (SRM) and the SRM transitions were the mass to charge ratio (m/z) of molecular cation to the daughter ion m/z 184, the specific phosphocholine group. The PE species were monitored using Selected Reaction Monitoring (SRM) and the SRM transitions were the mass to charge ratio (m/z) of molecular cation to the daughter ion at m/z minus 141, the specific ethanolamine group.

2.8.3. Data analysis

Software Xcalibur was used to get the peak area for all the lipid species. The internal standard calibration curves were used to calculate the relative concentration of all the PC and PE species in the samples.

2.9. PamGene PamStation sample preparation

Kinase activity was measured using serine-threonine kinases (STK) PamChip4 porous 3D microarrays and measured using the PamStation12 (PamGene International, 's-Hertogenbosch, The Netherlands). Substrates contained in each array are listed in Supplemental Table 1. Mouse livers were pooled and measured in triplicate across three chips simultaneously for STK, as previously described in [22—24]. This approach effectively deals with large batch effects across samples. It allows for the characterization of kinase activity only in the context of analytical variance. The pooled samples were lysed using M-PER Mammalian Extraction Buffer (Thermo Fischer Scientific, CAT#78503), Halt Phosphatase Inhibitor (Thermo Fischer Scientific, CAT#78428), and Protease Inhibitor Cocktail (Sigma, CAT#P2714). The samples were homogenized using TissueLyser LT (Qiagen). The protein concentration was measured in triplicate using Pierce BCA Protein assay (Thermo Fischer Scientific, CAT#23225). Samples were diluted to a final protein concentration of 2.5 μg/μl. Each array contained 1 μg of protein per sample for the STK chips. In the presence of adenosine triphosphate (ATP), kinase phosphorylation activity is quantified using fluorescently labeled antibodies to detect differential phosphorylation of 144 (STK) reporter peptides between experimental and control conditions, as previously described [25]. Evolve (PamGene) software uses a charge-coupled device (CCD) camera and light-emitting diode (LED) imaging system to record relative phosphorylation levels of each unique consensus phospho-peptide sequence every 5 min for 60 min as measured by peptide signal intensities recorded across 10, 20, 50, and 100 millisecond exposure times. Raw imaging data were exported for further data analysis and kinase mapping.

2.10. PamGene PamStation kinase data analysis

The images taken during the run were analyzed using BioNavigator (PamGene). Signal ratios are used to calculate fold change (FC) for each phosphopeptide sequence averaged across three replicates. Minimum threshold values were selected using cutoffs cited in previous literature [25—28]. These thresholds require differential phosphopeptide signals greater than or equal to 30% (FC $\geq$ 1.30 or FC $\leq$ 0.70) for differential phosphorylation to be considered. Linear regression slopes provide phosphorylation intensity signals used in differential analyses (e.g., experimental vs. control). Undetectable and/or nonlinear ($R2 < 0.80$) phosphopeptides are excluded from subsequent analyses. We performed upstream Kinase identification using Kinome Random Sampling Analyzer (K.R.S.A.) [29] and Upstream Kinase Analysis (U.K.A.) [30], as previously described in [25]. The kinase scores from the K.R.S.A. and U.K.A. are included in Supplemental Table 2 (males) and 3 (females). MEOW (measurements extensively of winners) plots, as described in [24], were used to interrogate individual kinase activities on substrates considering the confidence of the experimental versus the control groups using the equation: [Log2 Fold Change (FC) of kinase substrates * Δconfidence (experimental hits/mean hits of 2000 random sampling iterations)]. Data input files for STK runs available on the GitHub repository at the following (https://github.com/The-Hinds-Lab/Liver-Specific-Cpt1a-KO-Kinome-Analysis).

2.11. Real-time PCR analysis of gene expression

RNA extraction, cDNA synthesis, and quantitative real-time PCR was performed as previously described [16,17]. A small portion of frozen livers ($\sim$20 mg) were homogenized in 1 mL of QIAzol (Qiagen 79,306). After the addition of 200 μL of chloroform, phase separation occurred by centrifugation and the top layer was mixed with 400 μL of 75%

ethanol prior to running the sample over a RNeasy spin column (Qiagen, RNeasy Mini Kit). 500 ng of RNA was used as a template to synthesize cDNA (High Capacity cDNA Reverse Transcription Kit, Applied Biosystems). QPCR reactions were carried out using 2X SYBR green (Cowin Biosciences) and mRNA expression levels were calculated using the $\Delta\Delta$-Ct method on an Applied Biosystems (ABI) QuantStudio 7 Flex Real-Time PCR System. Primers used for qPCR are listed in Supplemental Table 4.

2.12. Bulk RNA-Sequencing

RNA was isolated using the RNeasy Mini kit (Qiagen) from livers of male and female, WT and LKO mice fed HFD for 15-weeks. The quantity and quality of the samples were determined using the Cytation 5 (BioTek) plate reader and Agilent 4150 Tape Station System, respectively, prior to submission to Novogene. The mRNA-seq libraries were prepared and sequenced on an Illumina HiSeq2500 platform, at a depth of 20 M read pairs (or 10 M/sample) by Novogene. After sequencing, the paired-end clean reads were aligned to the reference genome using Hisat2 v2.0.5. FeatureCounts v1.5.0-p3 was used to count the read numbers mapped to each gene, and the fragments per kilobase of transcript (FPKM) of each gene was calculated based on the length of the gene and read counts mapped to the gene.

Differential expression analysis was performed using the DESeq2 R package (1.20.0). The resulting p-values were adjusted using the Benjamini and Hochberg's approach for controlling the false discovery rate. Genes with an adjusted p-value $\leq$0.05 found by DESeq2 were assigned as differentially expressed. Gene ontology (GO) enrichment analysis of differentially expressed genes was implemented by the clusterProfiler R package. GO terms with corrected p-values <0.05 were considered significantly enriched by differential expressed genes. The clusterProfiler R package was also used to test the statistical enrichment of differentially expressed genes in KEGG pathways (https://www.genome.jp/keg/).

2.13. Immunoblotting

Whole liver ($\sim$20 mg) homogenates were solubilized in 1 mL of 1X ice-cold RIPA buffer (Cell Signaling) supplemented with 1X protease and phosphatase inhibitor cocktail (bimake.com). After two sequential centrifugation steps (13,000 rpm for 10 min), the supernatant was collected and protein was quantified using the Pierce™ Bicinchoninic Acid Protein (BCA) assay (ThermoFisher). For SDS-PAGE, 10 μg of protein was loaded and separated on 4—15% criterion TGX gels. Proteins were blocked with 5% milk and probed with antibodies listed in Supplemental Table 5. Images were taken on a ChemiDoc MP Imaging System (Bio-Rad) and quantification of blots were performed using ImageJ software (NIH).

2.14. TAG hydrolysis measurements

Triacylglycerol hydrolysis experiments were conducted as previously described [31]. A small piece of liver tissue was first homogenized in assay buffer containing 20 mM Tris-HCl, 150 mM NaCl, and 0.05% Triton X-100 (pH = 8.0). Lysates were spun at 15,000$\times g$ for 15 min and the infranatant was collected for a Pierce BCA protein assay. 50 μg of protein lysate was then brought up to 180 uL with assay buffer and added to a black, 96 well microtiter place on ice. The substrate resorufin ester (Sigma D7816) was prepared in 0.3 mg/mL of assay buffer, and 20 uL was then added to all samples. Kinetic readings were taken every 2 min at 530 nm excitation and 590 emission. Moles of resorufin ester hydrolyzed are calculated from a standard curve generated using free resorufin.

2.15. Transmission electron microscopy

A 1 mm × 3 mm piece of liver was fixed with 2.5% glutaraldehyde/4% paraformaldehyde in 0.2 M cacodylate buffer overnight at 4 °C. The sample was then washed 3 times with sodium cacodylate buffer (0.2 M, pH 7.3) at 5 min/wash. The buffer was removed, the samples were post-fixed with 1% Osmium Tetroxide (in H2O) for 60 min at 4 °C. The samples were washed 2 times with sodium cacodylate buffer for 5 min/wash, then rinsed with 2% Maleate buffer (pH 5.1) for 5 min. The buffer was changed to 1% uranyl acetate in Maleate buffer and stained for 60 min at room temperature (RT). After staining, the uranyl acetate was removed and washed with maleate buffer 3 times at 5 min each. Dehydration is followed by different concentrations of cold ethanol 30%, 50%, 75%, 95% 1X, 5 min/wash followed by 100% ethanol at RT 3 times for 10 min/wash. For the infiltration step, the 100% ethanol was removed, and 1:1 ethanol/eponate12 medium was added at RT overnight. The media was then removed and changed to pure eponate 12 medium for 4–6 h at RT. For embedding, the sample was placed into pure eponate 12 in a rubber mold and allowed to polymerize for 24 h in an oven at 62 °C. Ultra-thin sections (85 nm) were cut with diamond knife, stained with 10% uranyl acetate and lead citrate, and then observed with a Tecnai G2 SpiritBT electron microscope operated at 80 kV.

2.16. Statistical analysis

All graphs and statistical analyses were completed using GraphPad Prism 9.3.0. Data are expressed as ±SEM, unless otherwise noted in the figure legends. Differences were computed using two-way ANOVAs followed by a Tukey's multiple comparison *post hoc* analysis. When comparing two groups, a Student's *t*-test was utilized. Energy expenditure was calculated by analysis of covariance (ANCOVA) using body weight as a covariate [32]. P-values <0.05 were considered statistically significant. All figure legends contain the statistical analysis used for each panel of data.

3. RESULTS

3.1. Liver-specific deletion of CPT1a does not influence body weight or adiposity

To examine the mechanisms by which excess dietary fatty acids alter hepatic lipid metabolism in a sex- and CPT1a-dependent manner, we fed 6–8 week old male and female, *Cpt1a*-liver specific knockout (LKO) and littermate *Cpt1a*$^{F/F}$ (Control) mice a semipurified low-fat (LFD; 10% kcal fat) or high-fat diet (HFD; 60% kcal fat) for 15 weeks. An experimental scheme has been provided in Figure 1A. Mice were necropsied after a 16-hour fast to induce adipose tissue lipolysis and concomitant hepatic FAO (Figure S1A) [33]. To confirm successful deletion of *Cpt1a* in the liver, we measured *Cpt1a* RNA and protein levels in livers collected from LFD- and HFD-fed mice. Real-Time PCR (qPCR) analysis revealed a 70–80% reduction in *Cpt1a* RNA in male and female LKO mice fed LFD (Figure S1B) and HFD (Figure 1A). Immunoblotting followed by densitometry confirmed CPT1a protein levels were significantly reduced in LKO mice (Figures 1B–C, S1C–D). Previous reports have shown that another Cpt1 isoform, *Cpt1b*, may compensate for the loss of *Cpt1a* [34]. We then measured the relative expression of *Cpt1b* by qPCR and found it to be elevated with the loss of *Cpt1a* in male mice fed either a LFD (Figure S1E) or a HFD (Figure 1D). Female LKO mice exhibited increased *Cpt1b* gene expression with LFD feeding (Figure S1E) but was reduced in LKO mice fed a HFD, relative to control mice (Figure 1D). Despite relative compensatory changes in *Cpt1b* measured by qPCR, total read counts of the *Cpt1b* transcript by RNA-sequencing showed it is ∼10,000× lower than *Cpt1a* (Figure 2A

and B) and is undetectable by western blot (Figure S2C). Consistent with loss of the predominant Cpt1 isoform in the liver, male and female LKO mice displayed a 77% and 62% reduction in fasting serum β-hydroxybutyrate levels, a surrogate for hepatic FAO [35], upon LFD and HFD feeding, respectively (Figures 1E and S1F).

To determine if LKO mice exhibited changes in overall adiposity prior to dietary manipulation, we measured baseline adiposity in 6–8 week old control and LKO mice by Echo MRI. Baseline body weights were elevated in males compared to females, however loss of CPT1a in the liver had no impact on overall body weight (Figure S3A), fat mass (Figure S3B), or lean mass (Figure S3C) compared to their respective controls. Next, we measured body weights and adiposity in response to LFD- and HFD-feeding for 15-weeks. Control and LKO mice fed LFD had comparable increases in body weight (∼23–35% increase from baseline) and percent fat mass throughout the 15-week study, regardless of sex or genotype (Figure 3D and E). When challenged with HFD, male and female mice increased their body weight by ∼100% but no significant differences were observed across genotypes (Figure 1F). Consistent with baseline (Figure S3A–C), female mice had greater fat mass (∼41% fat mass) than male mice (∼34% fat mass) at the end of 15-weeks of HFD-feeding, independent of hepatic CPT1a (Figure 1G). Taken together, LKO mice had reduced hepatic CPT1a protein and ketone levels with fasting; however, there were no observable differences in adiposity or body weight gain in response to LFD- or HFD-feeding.

3.2. Liver-specific CPT1a deficiency alters food intake and total activity in female mice

Alterations in both substrates (free fatty acids; FFAs) and products (long chain acylcarnitines) of CPT1a have been associated with insulin resistance [36,37]. This prompted us to investigate whether liver-specific deletion of *Cpt1a* would affect systemic glucose tolerance and insulin sensitivity in mice. Following 10 weeks on diet, mice were fasted overnight and underwent a glucose tolerance test (GTT). In response to LFD, male and female LKO mice (Figure S4A) had improved glucose tolerance (significance by genotype = 0.0383) despite similar fasting glucose levels, as compared to control mice (Figure S4A–B). During insulin tolerance tests (ITT), male LKO mice appeared more resistant while female LKO mice were more sensitive to glucose uptake by exogenous insulin treatment (Figure 4C and D). Similar to LFD-feeding, HFD-fed LKO mice showed similar fasting glucose levels as control mice (Figure S5A); however, male LKO mice had significant lower fasting insulin levels (0.83 ± 0.39 ng/mL) as compared to male control mice (2.16 ± 1.0 ng/mL; Figure S5B). These reductions in fasting insulin levels drove improvements in the homeostatic model assessment for insulin resistance (HOMA-IR; Figure S5C), a surrogate marker for insulin resistance [38]. No changes in glucose or insulin sensitivity were observed from GTT and ITT, respectively, in HFD-fed LKO mice (Figure 5D and E).

We then utilized indirect calorimetry to examine the effects of liver-specific deletion of *Cpt1a* on metabolic parameters in male and female mice in response to HFD-feeding. Notably, control and LKO mice were challenged with an overnight fast during night 4 of the five-day experiment. Over the course of the 5-day experiment, male control and LKO mice exhibited no differences in cumulative food intake during the light and dark cycles (Figure S6A–C). Female LKO mice, however, consumed ∼10% more calories and were ∼20% more active than female control mice (significance by genotype = 0.0018 and 0.0122, respectively; Figure 6D–F; S7D-F). We then assessed energy expenditure using body weight as a covariate and observed female control and LKO mice exhibit similar degrees of energy expenditure across the light and dark cycles (Figure S8C). Taken together, female
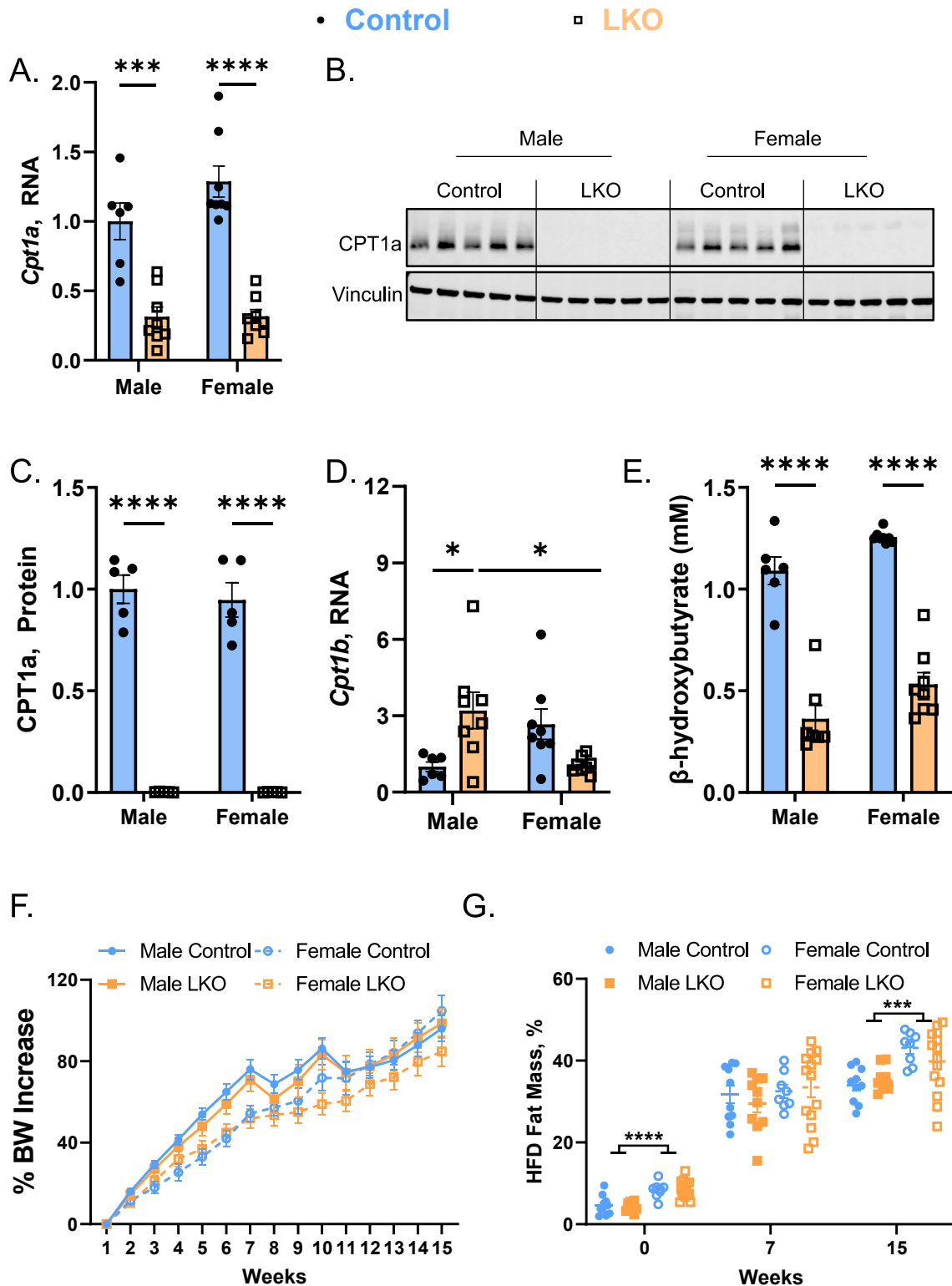
Figure 1: Liver-specific CPT1a Deletion Has No Effect on Body Weight in Response to HFD-Feeding. Male and female control and LKO mice were fed a HFD for 15-weeks. (A–C) Liver CPT1a RNA and protein levels were measured by qPCR (A; n = 6–8) and western blot (B; n = 5) followed by densitometry (C; n = 5), respectively. Vinculin is used as a loading control. (D) *Cpt1b* RNA levels were measured by qPCR from livers of HFD-fed male and female control and LKO mice (n = 6–8). For all qPCR analyses, housekeeping genes *Tbp* and *Hprt* were averaged and used for normalization. (E) β-hydroxybutyrate levels were measured from the plasma of fasted mice (n = 6–8). (F, G) Percent body weight (F) and fat (G) mass were recorded throughout the duration of the study (n = 8–14). Significance was determined by two-way ANOVA with Tukey's multiple comparison *post hoc* analysis. *P < 0.05; ***P < 0.001; ****P < 0.0001.

LKO had enhanced caloric intake and total activity as compared to their littermate controls.

3.3. Female CPT1a LKO mice exhibit panlobular microvesicular steatosis and exacerbation of liver injury in response to HFD-feeding

Hepatic steatosis, a hallmark feature of SLD, is defined by the accumulation of triacylglycerol and cholesterol esters in the core of cytosolic lipid droplets [39,40]. Hepatic lipid droplet accumulation can be driven by prolonged fasting (e.g. fasting-induced steatosis) and by overnutrition (e.g. HFD-feeding). We first assessed the impact of liver-specific *Cpt1a*-deficiency on fasting-induced steatosis with LFD-feeding and found that male and female LKO mice had increased liver weights and hepatic triglycerides, as compared to their respective controls (Figure 9A and B) [41]. Meanwhile, hepatic cholesterol levels were significantly increased only in female LKO mice (Figure S9C), while no differences were observed in serum alanine aminotransferase (ALT) levels, a marker of liver injury (Figure S9D). In response to HFD, female control mice were protected against diet-induced liver injury and had reduced liver weights (34.5%), hepatic triglycerides (38.9%), and serum ALT levels (67.9%) as compared to male control mice (Figure 2A–D). Female LKO mice, however, completely lost this protection characterized by increased liver weights (53.9%), hepatic triglycerides (141.3%) and cholesterol (129.1%), and serum ALT levels (67.9%), as compared to female control mice (Figure 2A–D). Notably, male LKO mice had comparable liver weights and hepatic lipids (triglycerides, cholesterol), as well as reduced ALT levels (−42.6%) as compared to male control mice (Figure 2A–D).

The liver lobule can be broken down into anatomical zones based off their metabolic function. Hepatocytes occupying the periportal region (zone 1) are exposed to oxygen-rich blood flow and undergo greater rates of FAO [42,43]. Hepatocytes occupying the pericentral region (zone 3) are exposed to more hypoxic-like conditions and undergo more triglyceride synthesis [42,43]. The accumulation of LDs observed in SLD typically affects pericentral hepatocytes (zone 3). Given FAO is highly active in periportal hepatocytes, we asked whether we could drive LD accumulation in periportal hepatocytes. To assess this, we stained liver sections with hematoxylin and eosin (Figure 2E,F) and blindly quantified the size and total number (per nuclei) of 17,473 LDs across the periportal–pericentral axis. Male control mice displayed significant pericentral steatosis (Figure 2H) but were largely free from lipid droplet accumulation in periportal hepatocytes (Figure 2G). Male LKO mice displayed slight (albeit not significant) periportal steatosis, while pericentral steatosis was unaffected relative to male control mice (Figure 2E–H). Female control mice were protected from diet-induced LD accumulation as compared to male control mice; however, LKO mice displayed diffuse, panlobular microvesicular steatosis across the entire periportal–pericentral axis (Figure 2E–H). Consistently, female LKO mice had increased total LD number (Figure 2G,H) and a greater propensity to accumulate smaller LDs (37% of LDs within 5–10 μm) in the pericentral zone, as compared to female control mice (27.5% of LDs within 5–10 μm; Figure 10A and B). Further, transmission electron microscopy revealed significant LD accumulation in female LKO mice as compared to female control mice (Figure 2I). Taken together, female mice are protected from diet-induced SLD in a *Cpt1a*-dependent manner, while male mice are largely unaffected by *Cpt1a*-deletion in response to HFD-feeding.

3.4. Choline- and DHA-containing phospholipids are selectively reduced in livers from female LKO mice

The LD core is surrounded by a phospholipid monolayer consisting of primarily (>90%) phosphatidylethanolamine (PE) and phosphatidylcholine (PC) [44,45]. Given that female LKO mice accumulated many small LDs (Figure 2I), we reasoned that phospholipid levels would also be affected in these mice. Utilizing an untargeted lipidomics approach by liquid chromatography-tandem mass spectrometry (LC-MS/MS), we observed similar levels of all major phospholipid species (PE, PC, phosphatidylserine [PS], phosphatidylinositol [PI], phosphatidylglycerol [PG], and phosphatidic acid [PA]) in male control and LKO mice (Figure S11A). To our surprise, however, female LKO mice had decreased PC levels at the expense of both PE and PG in the liver (Figure 3A). This lipidomics approach allows for semi-quantitation of lipid species, so we validated our untargeted analysis by quantifying the total mass of PC in livers from HFD-fed mice using a Folch-based extraction followed by an enzymatic assay containing PC standards. Consistently, female LKO mice had 9.9 ± 1.74 (mg PC/g liver) relative to female control mice 13.9 ± 3.02 (mg PC/g liver), a 28.3% reduction in the total mass of hepatic PC (Figure S11B). The ratio of cellular PC to PE is critically important for maintaining LD growth and stability, and is tightly controlled by the phosphatidylethanolamine N-methyltransferase (PEMT) enzyme which facilitates PC synthesis from PE [44,46,47]. We observed a significant 35% reduction in the ratio of total PC to PE (Figure 3B), which is associated with reduced PEMT gene (1.5 fold) and protein (4-fold) levels (Figure 3C–E) in female LKO mice relative to control mice. These data are consistent with reduced hepatic PC synthesis and accumulation of PE in female LKO mice.

Aside from the total phospholipid pool, we next asked if CPT1a deficiency would alter the acyl-CoA composition of PE and PC. Male and female LKO mice exhibited increased MUFA (34:1, 34:2, 36:1, 36:2)-, ω6-PUFA-(36:3, 38:4)-, and EPA (38:5)-containing PE (Figure 3F) and PC (Figure 3G), while DHA-containing (38:6, 40:6) phospholipids were selectively reduced (Figure 3F,G). Female LKO mice exhibited the most profound differences in PUFA-containing phospholipids, particularly the significant reductions in 38:6 PE ($P = $ 2.1E-08; Figure 3F) and PC ($P = $ 2.9E-04; Figure 3G) levels in the liver. Altogether, female LKO mice had increased hepatic PE levels at the expense of PC, which coincided with decreased PEMT protein levels in the liver. Moreover, both male and female LKO mice had increased MUFA-containing phospholipids at the expense of DHA-containing phospholipids, which tended to be more prominent in LKO females.

3.5. MUFA-containing phospholipids are increased at the expense of DHA-containing phospholipids in LD fractions collected from LKO mice

Given the shift towards MUFA-containing PE and PC in whole cell lysates (Figure 3), we asked whether these changes were also occurring within the LD phospholipid monolayer. We first isolated LDs from HFD-fed control and LKO mice by sucrose gradient centrifugation [17]. Using non-LD and LD fractions, we immunoblotted for LD (perilipin 2 [PLIN2], PLIN5), mitochondria (voltage-dependent anion channel, VDAC), and cytosolic (glyceraldehyde 3-phophshate dehydrogenase, GAPDH) proteins. We confirmed the presence of PLIN2 and PLIN5 on LD-fractions, while these fractions were largely absent of the mitochondrial and cytosolic proteins, VDAC and GAPDH, respectively (Figure 4A). Both PLIN2 and PLIN5 were more abundant on LD-fractions from female LKO mice suggesting more PLIN2 and 5 protein were coating these LDs in female LKO mice (Figure 4A). We then extracted lipids from the LD fractions and quantified the acyl-CoA composition of PE and PC using a previously established targeted LC-MS/MS method [17]. Consistent with our observation in whole liver lysates (Figure 3), male and female LKO mice had increased MUFA-
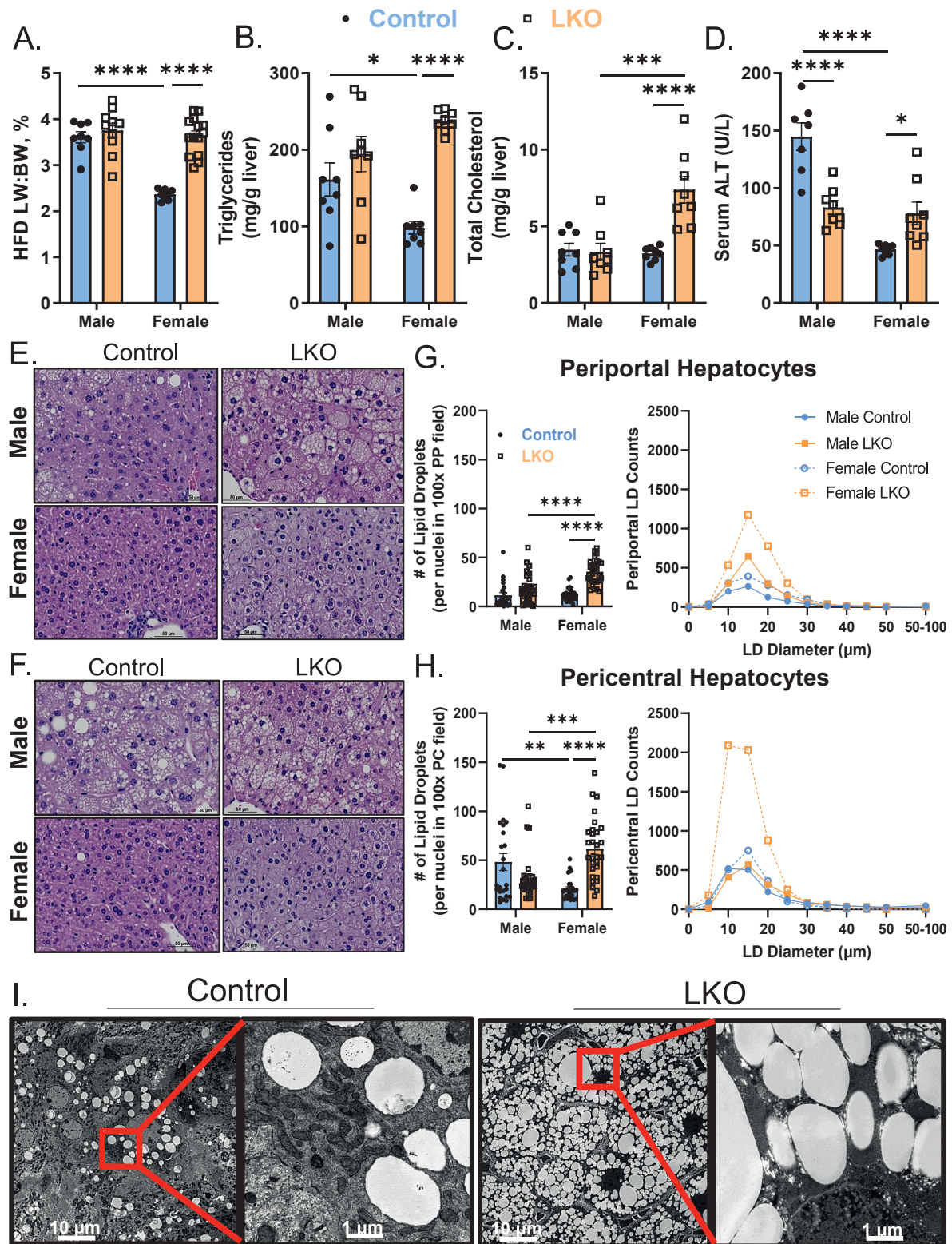
Figure 2: Female LKO Mice Develop Exacerbated Steatosis and Liver Dysfunction in Response to HFD-Feeding. Male and female control and LKO mice were fed a HFD for 15-weeks. (A—C) Liver weights normalized to body weight (A; LW:BW, %; n = 8—14), and hepatic triglycerides (B; n = 8) and total cholesterol (C; n = 8) levels were quantified enzymatically. (D) Serum ALT levels were quantified (n = 7—8). (E, F) Representative Oil Red O staining to assess neutral lipid accumulation across groups. The scale bar (50 μm) is embedded within the lumen of the portal (E) or central (F) veins in the corner of each image. Total number of lipid droplets (# lipid droplets/nuclei in 100X field) and their respective diameters were quantified in periportal (G) and pericentral hepatocytes (H). A total of 17,473 lipid droplets were quantified across 19 mice. (I) Transmission electron microscopy was completed on livers collected from HFD-fed female control and LKO mice (scale bars = 10 μm on left image and 1 μm on right image). Significance was determined by two-way ANOVA with Tukey's multiple comparison *post hoc* analysis. *P < 0.05; **P < 0.01; ***P < 0.001; ****P < 0.0001.
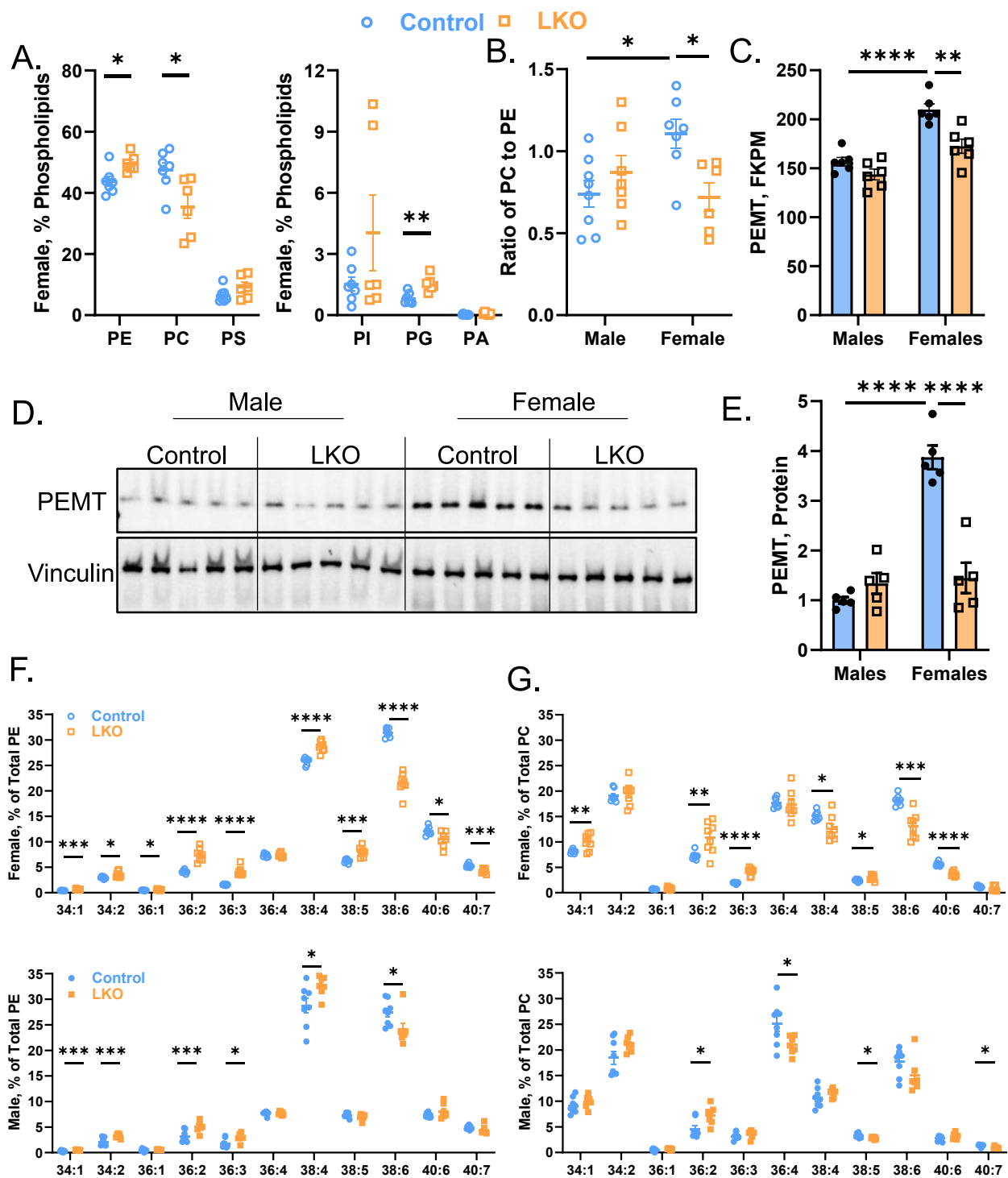
Figure 3: Female LKO Mice Have Increased PE and MUFA-Containing Phospholipids in the Liver. Male and female control and LKO mice were fed a HFD for 15-weeks. (**A**) Whole cell liver lysates were subjected to LC-MS/MS based lipidomics. Phospholipid species (PE, PC, PS, PI, PG, PA) displayed as percent (%) of total phospholipids (n = 6−8). (**B**) A ratio of total PC to PE across the four groups (n = 6−8). (**C**) Total read counts of *Pemt* from bulk RNA-sequencing data provided in Figure 6 (FPKM = fragments per kilobase million; n = 6). (**D, E**) Immunoblotting (**D**) followed by densitometry (**E**) for PEMT protein (n = 5). Vinculin is used as a loading control. (**F, G**) The fatty acyl composition of PE (**F**) and PC (**G**) from female (top) and male (bottom) mice. All data are presented as % of total phospholipid (n = 7−8). Significance was determined by an unpaired Student's t-test (panels A, F, G) or by a two-way ANOVA with Tukey's multiple comparison *post hoc* analysis (panels B, C, E). *P < 0.05; **P < 0.01; ***P < 0.001; ****P < 0.0001.
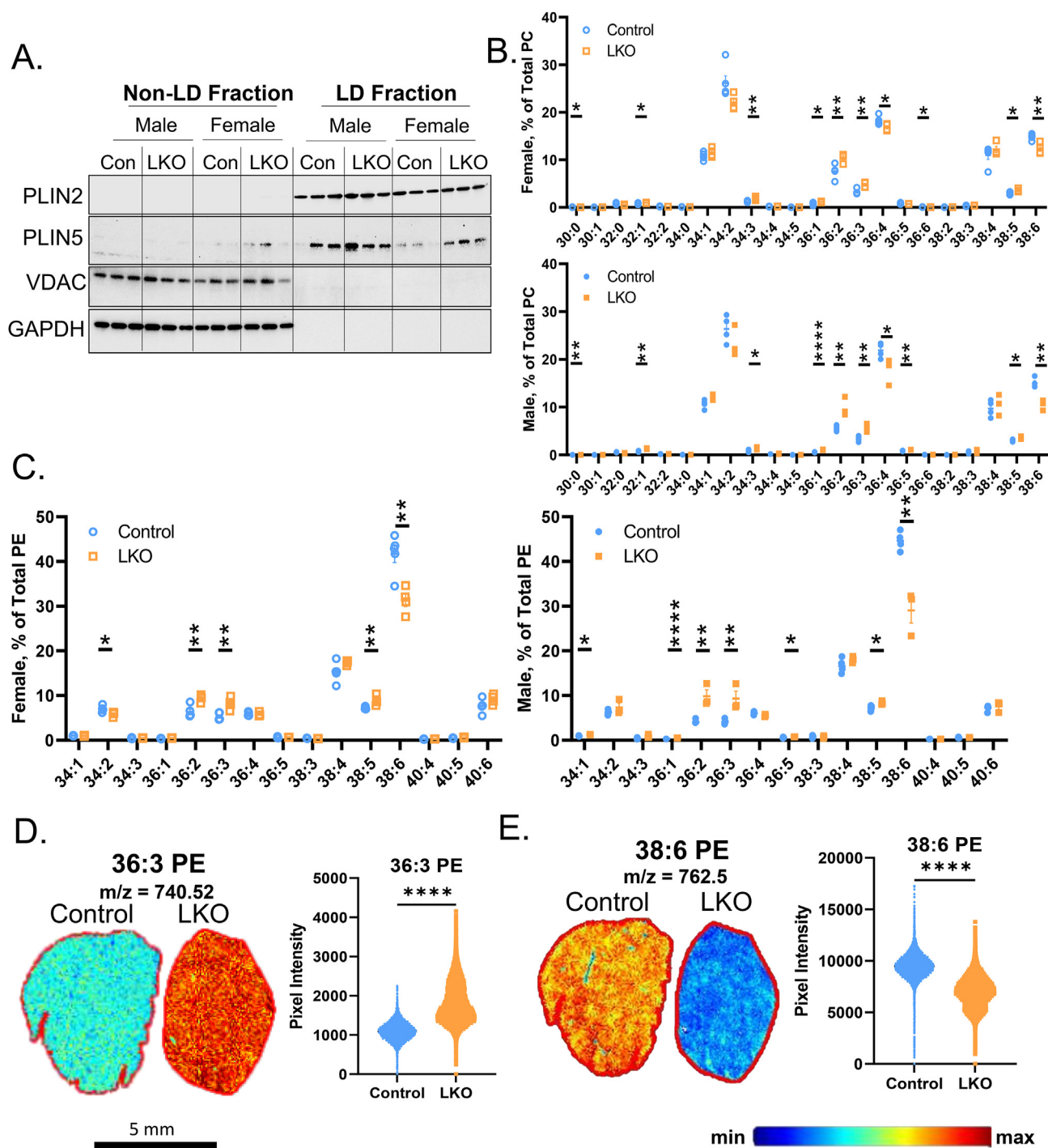
Figure 4: Lipid Droplets Isolated from LKO Mice Have Increased MUFA-Containing Phospholipids. Male and female control and LKO mice were fed a HFD for 15-weeks. (**A**) Non-LD and LD fractions were isolated from livers and immunoblotted for PLIN2, PLIN5, VDAC, and GAPDH (n = 3). (**B, C**) Lipid droplet fractions were subjected to targeted semi-quantification of PC (**B**) and PE (**C**; n = 3−5). (**D, E**) MALDI-MSI was completed on whole livers from female control and LKO mice (n = 4). A representative spatial map and pixel intensity are shown for 36:3 PE (**D**) and 38:6 PE (**E**). Significance was determined by unpaired Student's t-tests. *P < 0.05; **P < 0.01; ***P < 0.001; ****P < 0.0001.

containing PC (Figure 4B) and PE (Figure 4C) at the expense of DHA-containing phospholipids, particularly 38:6 PE (Figure 4B,C).

Phospholipids exhibit varying spatial intensities across the periportal—pericentral axis in response to genetic- and dietary manipulation [42,48]. While periportal hepatocytes are thought to undergo greater FAO rates, they also contain more arachidonic acid- and DHA-

containing phospholipids (e.g. 38:6 PC) [42,48]. Therefore, we asked whether the panlobular microvesicular steatosis observed in female LKO mice may lead to changes in the spatial distribution of these key MUFA- and PUFA-containing phospholipids. Utilizing MALDI-MSI technology, we observed that female LKO mice had significantly increased 36:3 PE intensity, while the intensity for the DHA-containing

phospholipid, 38:6 PE, was significantly reduced across the entire liver lobule (Figure 4D). While there was a tendency for 38:6 PE to exhibit spatial localization across the liver lobule in control mice, the intensity was dramatically reduced across the entire lobule in both male and female LKO mice (Figure 4D, S12). A compilation of all MALDI-MSI spatial maps for 36:3 PE and 38:4 PE across males and females has been provided in Figure S12. Collectively, whole cell lysates and LDs isolated from LKO mice favor MUFA-containing at the expense of DHA-containing PE and PC, which appears to be pan-lobular rather than spatially localized across the periportal−pericentral axis.

3.6. PPAR signaling and PUFA biosynthetic genes are upregulated in LKO mice

To attempt to tease out the mechanisms explaining the sexually dimorphic response to *Cpt1a* deficiency, we completed bulk RNA-sequencing on whole livers from HFD-fed male and female mice. We identified 577 (male) and 748 (female) genes that met pre-determined statistical (p-adjusted value ≤ 0.05) and effect size cut-offs (Log2 normalized fold-change [FC] of ±0.58). Partial least squares-discriminant analysis showed that the transcriptome of LKO mice was profoundly different from that of WT mice (both in males and females), accounting for up to 12.16% on PC2 (Figure S13A). Moreover, sex alone accounted for up to 24.61% of the total variation on PC1 between male and female mice (Figure S13A). The most downregulated gene in both male and female LKO mice was *Cpt1a*, while several other genes involved in *de novo* lipogenesis (*Srebf1*, *Acly*) and carbohydrate metabolism (*Khk*, *Tkfc*, *Pklr*, *Pygl*) were significantly downregulated compared to control mice (Figure 5A,B). Laminin subunit beta-3 (*Lamb3*), which is involved in Akt-mediated tumorigenesis [49], was the most significantly upregulated (Log$_2$ FC = 2.39; Padj = 2.05E-73) gene in response to LKO in male mice. In female LKO mice, the most significantly upregulated gene (Log$_2$ FC = 3.61; Padj = 1.18E-58) was cell death-inducing DFFA-like effector C (*Cidec*), a gene encoding a LD-tethering protein involved in the fusion and growth of LDs [50]. Genes encoding proteins that influence LD turnover (*Plin2*, *Hilpda*, *G0S2*) and fatty acid metabolism (*Acot2*, *Cyp4a14*, *Cyp4a12*) were collectively upregulated in LKO mice across both sexes (Figure 5A,B). Notably, inflammatory genes (*Ly6d*, *Mmp12*, *Cxcl2*) were selectively upregulated only in female LKO mice (Figure 5B), likely contributing to the worsened liver injury in these animals (Figure 2D).

To determine pathways differentially affected by *Cpt1a*-deletion in the liver, we completed a Kyoto Encyclopedia of Genes and Genomes (KEGG) enrichment analysis for both male and female mice. The top 5 dysregulated pathways comparing male control and LKO mice were related to peroxisome proliferator-activated receptor (PPAR) signaling, fatty acid degradation, arachidonic acid metabolism, fatty acid elongation, and retinol metabolism (Figure 5C). Similarly, in female mice, the top 5 pathways affected were related to retinol metabolism, chemical carcinogenesis, linoleic acid metabolism, and PPAR and insulin signaling (Figure 5D). Since both male and females had enrichment of PPAR signaling pathways, we measured individual PPAR isoforms (α, δ, γ1, γ2) using normalized read counts from RNA-sequencing and by qPCR. Along with impairments in long chain FAO with *Cpt1a*-deficiency, RNA levels of the major transcription factor controlling FAO gene transcription, PPARα, was elevated in both male and female LKO mice (significance by genotype = 0.0005; Figure S13B). Moreover, only female LKO had significant elevations in PPARγ1 (Figure S13B), while PPARδ and PPARγ2 were unaffected. Aside from PPAR-signaling, the KEGG enrichment analysis also identified several pathways related to PUFA metabolism. The synthesis of PUFAs, such as DHA, are mediated by a series of reactions that involve

the desaturation and elongation of substrate lipids. The enzymes catalyzing these reactions include members of the fatty acid desaturase (*Fads1, 2*) and elongase gene families (*Elovl2, 5*). We examined normalized read counts of PUFA biosynthetic genes in livers collected from female control and LKO mice fed a HFD. Despite significant reductions in DHA-containing phospholipids in both whole liver lysates (Figure 3F,G) and in LDs (Figure 4B,C), the biosynthetic enzymes *Elovl5*, *Fads1*, and *Elovl2* were transcriptionally elevated in LKO mice relative to control mice (Figure 5E; S13C).

Given the shift from DHA to MUFA-containing phospholipids, we also measured RNA levels of genes known to regulate the acyl-CoA composition of phospholipids. The long-chain acyl-CoA synthetase 4 (*Acsl4*) gene facilitates the synthesis of long-chain PUFA-CoAs for esterification into phospholipids, albeit with a preference for arachidonic acid and ω3-PUFAs [51]. In female LKO mice, *Acsl4* gene expression was significantly elevated as compared to control mice (Figure 5F). No changes were observed in RNA levels of 1-acyl-*sn*-glycerol-3-phosphate acyltransferase (*Agpat3*) or lysophosphatidylcholine acyltransferase (*Lpcat3*), two genes shown to facilitate DHA [52]- and arachidonic acid [53]-incorporation into PE lipids, respectively (Figure S13C). The *sn*-1 position of PE contains saturated fatty acids (SFAs) or MUFAs, and recent work identified transmembrane proteins containing TRM-Lag1p-CLN8 domains 1 and 2 (*Tlcd1, 2*) as selective inducers of MUFA incorporation into *sn*-1 position of PEs [54]. Consistent with previous reports that *Tlcd1* and *Tlcd2* increase MUFA-PEs and drive worsened liver injury in mice [54], female LKO mice exhibited elevated *Tlcd1* RNA levels as compared to female control mice (Figure 5F; S13C). Altogether, male and female LKO mice respond to *Cpt1a*-deletion by upregulating PPARα signaling (and PPARγ1 in females) and its downstream targets, some of which are involved in LD hydrolysis (*Cidec*, *Plin2*, *G0s2*; Figure 5A−D) [55,56]. Moreover, genes involved in PUFA biosynthesis (*Elovl5*, *Fads1*, *Elovl2*) and in MUFA incorporation into PE (*Tlcd1*) were also elevated in female LKO mice (Figure 5E).

3.7. PKA signaling and triglyceride hydrolysis is impaired in LKO mice

To identify altered signal transduction that might influence downstream lipid and gene expression changes observed in LKO mice, we quantified the activity of 144 serine/threonine kinases (STK) in liver samples from HFD-fed male and female mice using PamGene technology in real-time [22,25]. We determined individual substrate phosphorylation from the PamGene analysis into heatmaps showing the top peptides that exhibited differential phosphorylation compared to controls (Figure 14A and B). We then used bioinformatics to identify upstream kinases responsible for the observed difference in phosphorylation across all peptides. The activity of protein kinase A (PKA) was one of the most repressed STKs in LKO mice in both male and female mice. Peacock plots (Figure 6A; **S15A**), which show the confidence of our bioinformatics analysis relative to the number of random sampling over 2000 iterations and overall kinase activity across all PKA-peptides [22,25] (Figure 6B; S15B), demonstrate with high confidence that PKA activity was impaired in both LKO groups. A major role of PKA during fasting is to phosphorylate proteins involved in the lipolytic machinery of LDs, including perilipins and hormone sensitive lipase (HSL) in adipocytes. Individual peptides were then compiled in a waterfall plot across male (Figure 6C) and female mice (Figure S15C), and we discovered the hormone sensitive lipase (HSL) peptide (encoding serine 950, 951, and threonine 955) and the β2-adrenergic receptor (β2-AR) peptide (encoding serine 345 and 346) was significantly reduced in male LKO but not female LKO mice (Figure 6C; S15C). We then immunoblotted for perilipins (PLIN2, PLIN5), lipases
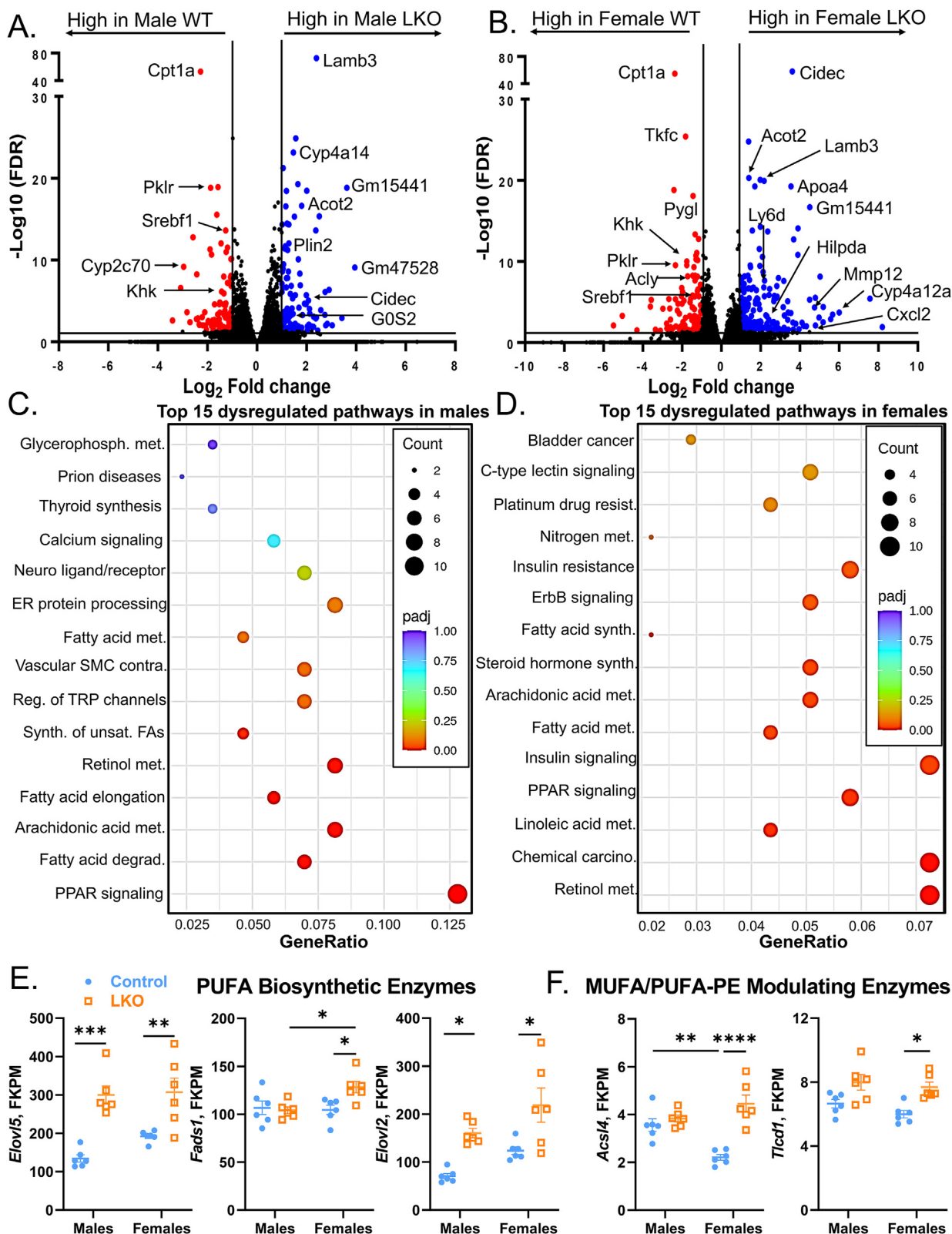
Figure 5: PPAR Signaling and Lipid Droplet Genes Are Elevated in LKO Mice. Bulk RNA sequencing was completed on the livers of male and female HFD-control and LKO mice. (**A, B**) Volcano plots in males (**A**) and females (**B**) highlighting all genes increased (in blue) or decreased (in red) with *Cpt1a*-deficiency. The horizontal black bar denotes the significance cutoff FDR = 0.05. The vertical black bars denote a minimal threshold for the effect size of 1.5 (Log2 fold change = ±0.58). (**C, D**) KEGG analysis dot plots for the top 15 dysregulated pathways in WT and LKO male (**C**) and female (**D**) mice. (**E, F**) Total read counts (in FPKM) for genes involved in the biosynthesis of PUFAs (**E**; *Elovl5*, *Fads1*, *Elovl2*) and fatty acyl remodeling of phospholipids (**F**; *Acsl4*, *Tlcd1*). Significance was determined by a two-way ANOVA with Tukey's multiple comparison *post hoc* analysis (panels E, F). *$P < 0.05$; **$P < 0.01$; ***$P < 0.001$; ****$P < 0.0001$.
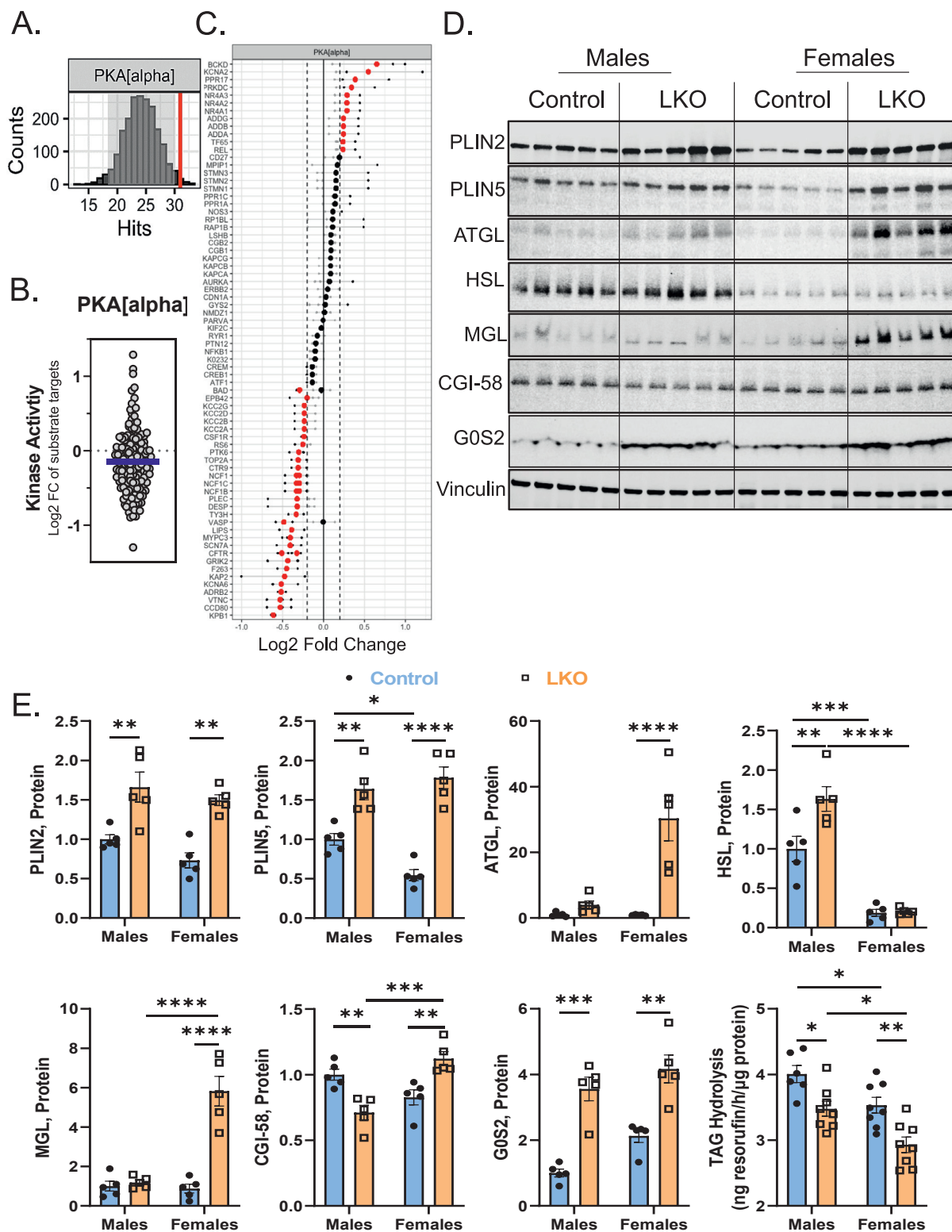
Figure 6: PKA Signaling and Triglyceride Hydrolysis Are Impaired in LKO Mice. A serine-threonine kinome analysis was completed on pooled liver samples from male HFD-fed control and LKO mice. A total of 6 mice per genotype were pooled and ran in triplicate on the PamGene PamStation. (**A**–**C**) PKA peacock (**A**), MEOW (**B**), and substrate waterfall plots (**C**) are presented comparing male control and LKO mice. The waterfall plot shows all known peptides that are phosphorylated by PKA and the extent by which their phosphorylation, in real-time, is increased or decreased (in red) with *Cpt1a*-deficiency. (**D**, **E**) Immunoblotting (**D**) followed by densitometry (**E**) for proteins (PLIN2, PLIN5, ATGL, HSL, MGL, CGI-58, G0S2) associated with regulating the size and turnover of LDs (n = 5). Vinculin is used as a loading control. (**F**) Triglyceride hydrolysis was completed using liver lysates from HFD-fed control and LKO mice using resorufin ester as substrate (n = 8). Significance was determined by a two-way ANOVA with Tukey's multiple comparison *post hoc* analysis. *P < 0.05; **P < 0.01; ***P < 0.001; ****P < 0.0001.

(adipose triglyceride lipase, ATGL; HSL, monoacylglycerol lipase, MGL), and lipase co-regulators (comparative gene identification 58, CGI-58; G0/G1 switch 2, G0S2) known to regulate LD lipolysis (Figure 6D). Consistent with changes at the RNA level (Figure 5), both male and female LKO mice had elevated PLIN2 and PLIN5 protein (Figure 6D,E). Total protein levels of ATGL, HSL, and MGL were largely unchanged in male LKO mice; however, female LKO mice had elevated ATGL ($\sim$30-fold) and MGL ($\sim$6-fold) protein levels, relative to female control mice (Figure 6D,E). Protein levels of the PPARα-target gene [57] and potent inhibitor of ATGL [58], G0S2, was also elevated (4-fold) in male and female LKO mice (Figure 6D,E). Consistent with impaired PKA signaling and increased protein levels of PLIN 2, 5, and G0S2, triglyceride hydrolysis was reduced in mice lacking *Cpt1a* in the liver (Figure 6E).

4. DISCUSSION

Here we report a novel role for CPT1a controlling sexually dimorphic SLD. First, we show that ablation of CPT1a in the liver of male mice promotes modest (although not significant) LD accumulation in periportal hepatocytes while total hepatic lipids (triglycerides, cholesterol) across the lobule were not different compared to male control mice. In fact, male LKO mice were protected from liver dysfunction (via ALT levels) compared to control mice. However, female control mice were largely protected from diet-induced liver dysfunction, which was completely lost in female mice lacking CPT1a in the liver. The exacerbation of SLD in female LKO mice was characterized by the accumulation of LDs within periportal and pericentral hepatocytes, consistent with significant elevations in triglycerides, cholesterol, and circulating ALT levels. Estrogen has been shown to stimulate FAO [59] and *Cpt1a* gene transcription via the estrogen receptor α [60]. It is plausible that estrogen mediates its hepatoprotective properties through a CPT1a-dependent FAO mechanism. However, we did not detect differences in CPT1a RNA or protein levels across male and female mice. Given that CPT1a activity is subjected to allosteric regulation by malonyl-CoA, future studies should determine if CPT1a enzymatic activity is regulated in a sexually dimorphic manner.

Next, we show that *Cpt1a* deficiency in female mice is associated with alterations in the total phospholipid pool from PC to PE, as well as the acyl-CoA composition of these two major phospholipids. The PEMT enzyme facilitates the methylation of PE to generate PC, accounting for $\sim$30% of total liver PC biosynthesis in mammalian hepatocytes, while the remaining $\sim$70% of PC is synthesized by the conversion of choline to PC [61,62]. PEMT confers specificity for PUFA-containing PE as a substrate for PC synthesis, while MUFA-containing PCs tend to be derived largely from the CDP-choline pathway [61,63]. A reduction in PEMT has been shown to deplete hepatic and plasma DHA-containing PC [64], promote steatosis, inflammation, and fibrosis in mouse models of SLD [65–67], and associate with an increased risk of worsened liver dysfunction in humans [68,69]. Notably, PEMT is responsive to estrogen due to three evolutionarily conserved estrogen regulatory motifs within the promoter [70], and loss of ovarian sex hormones by ovariectomy promotes SLD and reduces *Pemt* gene expression in the liver [71]. These publications largely support our findings where we show female LKO lose their protection from diet-induced SLD, which associates with lower PEMT protein and PC:PE ratios compared to female control mice. Given that PEMT tracks with the severity of SLD observed in control and LKO mice, it is plausible that PEMT drives the sexually dimorphic phenotype observed in these animals. Further, male and female LKO mice have reduced DHA-containing PC and PE, indicating other mechanisms independent of PEMT are likely driving the shifts in acyl-CoA phospholipid composition.

To further understand how *Cpt1a* shapes phospholipid metabolism, we measured the expression of genes involved in the PUFA-biosynthetic pathway. Despite reductions in DHA-containing phospholipids, we observed significant increases in the fatty acid elongase gene family (*Elovl5*, *Elovl2*). The ELOVL2 enzyme facilitates the elongation of 20- and 22-carbon PUFAs [72], while ELOVL5 has a broader fatty acid specificity [73]. Depletion of DHA, through genetic deletion of ELOVL5 or AGPAT3, drives SLD via activation of sterol response element binding transcription factor-1 (SREBP1)-mediated *de novo* lipogenesis [52,73]. On the contrary, supplementation of DHA strongly suppresses SREBP1 activation [73,74]. Given this negative feedback loop between DHA and SREBP1, we expected an increase in *Srepf1* and its downstream target genes, but *Srebf1* was consistently downregulated across male and female LKO mice, as were its canonical target genes *Acly* and *Fasn*. Given that this pathway is also positively regulated by insulin levels [75], the low insulin levels observed in LKO mice likely contribute to the reductions in lipogenic gene expression observed in these animals.

Aside from reduced SREBP1-mediated lipogenesis, our studies show that loss of CPT1a in the liver of male and female mice stimulates PPAR-signaling. We found that the PPARα isoform, which transcriptionally regulates genes involved in peroxisomal biogenesis and fatty acid metabolism, was elevated across male and female LKO mice. This is consistent with other reports in skeletal muscle showing compensatory increases in peroxisomal FAO in response to impaired mitochondrial FAO [76]. Further, an increase in peroxisome and LD number can be driven by MUFA supplementation, which in turn elevates the phospholipid MUFA:PUFA ratio and reduces the capacity for lipid oxidation [77]. On the contrary, impaired peroxisomal β-oxidation promotes the accumulation of PUFA-CoAs and represses large LD formation [78]. Therefore, enhanced PPARα signaling in LKO mice may accelerate DHA catabolism in peroxisomes leading to a shift in MUFA:PUFA-containing phospholipids in the LD monolayer, which results in smaller and more stable LDs.

Another key observation in female LKO mice was the significant elevation in *Pparγ1* RNA, which coincided with significant upregulation of *Cidec*, an established PPARγ target gene [79]. While PPARγ has historically been studied in adipose tissue, laboratories have shown that gain- and loss-of-function of PPARγ in the liver exacerbates and ameliorates diet-induced liver dysfunction [80,81], which is mediated, in part, by *Cidec* [79]. CIDEC is an LD-associated protein that facilitates the transfer of neutral lipids from smaller to larger LDs, thereby inhibiting lipolysis and controlling the expansion of these organelles [50]. Counterintuitive to its role in LD expansion, forced expression in the liver phenocopies the histopathology observed in female LKO mice — the accumulation of small LD vacuoles throughout the liver lobule [79]. Future studies are required to fully understand the role of *Cidec* in mediating microvesicular steatosis, a phenotype observed in individuals with impaired FAO [82].

To assess which signaling pathways might be altered with CPT1a ablation, we performed an unbiased characterization of STK activity in male and female mice. This analysis revealed significant suppression of cyclic adenosine monophosphate (cAMP)-dependent protein kinases, including protein kinase X (PRKX) and PKA in LKO mice. PKA functions as a heterotetramer which consists of 2 regulatory and 2 catalytic subunits, one of which is PRKX. An increase in intracellular cAMP, as observed during fasting, results in a conformational change of the protein leading to activation and subsequent phosphorylation of lipolytic proteins, including PLIN5 [83] and HSL [84], to drive LD catabolism. Inhibition of this pathway further promotes the accumulation of LDs in mice [85]. Consistent with reduced PKA activity, we observed significant reductions in triglyceride hydrolysis from liver lysates of LKO mice. This

reduction in hydrolysis can be attributed to loss of PKA activity and an increase in protein of known lipase inhibitors (PLIN2, PLIN5, G0S2), despite significant elevations in lipases themselves (ATGL, MGL). Collectively, a reduction in the PKA-mediated liberation of fatty acids from LDs likely serves as a negative feedback loop to protect hepatocytes from lipotoxicity during periods of impaired FAO.

It is important to note that some of the results highlighted here are not in complete agreement with a previous study showing the impact of liver-specific CPT1a-deficiency on SLD in mice. The manuscript by Sun et al. showed male CPT1a LKO mice had significantly lower body weight, and improved glucose and insulin tolerance in response to a 45% kcal from fat HFD [34]. While we were unable to replicate the lowering of body weight in LKO mice, we did observe significant reductions in circulating insulin levels in male LKO mice fed a 60% kcal from fat HFD, consistent with improvements in insulin sensitivity. Other notable differences include the observation that male LKO mice had significant elevations in hepatic triglycerides in response to HFD feeding [34]. In our studies, we did observe slight periportal steatosis in male LKO mice; however, hepatic lipid data from male mice were variable and insignificant compared to male control mice. In the previous report, female mice were not included, and it is unclear if mice were necropsied in the fed or fasted state [34]. Overall, while many of the phenotypes described by Sun et al. [34] was replicated here; a few distinct differences were noted and should be considered moving forward.

In this study, we show that female mice are dependent on CPT1a-mediated FAO for protection from HFD-induced SLD. The exacerbation of SLD observed with CPT1a deficiency in female mice is associated with significant reductions in hepatic PC synthesis via the PEMT-dependent pathway. Modulation of PPARα and PKA signaling pathways may serve as compensatory mechanisms to protect hepatocytes from lipotoxicity in the face of impaired FAO. Future studies should consider sexually dimorphic responses to FAO when designing more personalized therapeutics for the management of SLD.

AUTHOR CONTRIBUTIONS

Mikala M. Zelows: Conceptualization, Methodology, Validation, Formal analysis, Investigation, Data Curation, Writing — Original Draft, Writing — Review & Editing, Visualization. **Corissa Cady**: Investigation, Writing — Review & Editing. **Nikitha Dharanipragada**: Methodology, Formal analysis, Investigation, Data Curation, Writing — Review & Editing. **Anna Mead**: Methodology, Formal analysis, Investigation, Data Curation, Writing — Review & Editing. **Zachary Kipp**: Methodology, Software, Validation, Formal analysis, Investigation, Data Curation, Writing — Review & Editing. **Evelyn Bates**: Methodology, Software, Validation, Formal analysis, Investigation, Data Curation, Writing — Review & Editing. **Venkateshwari Varadharajan**: Formal analysis, Data Curation, Writing — Review & Editing. **Rakhee Banerjee**: Formal analysis, Data Curation, Writing — Review & Editing. **Se-Hyung Park**: Investigation, Writing — Review & Editing. **Nathan R. Shelman**: Formal analysis, Data Curation, Writing — Review & Editing. **Harrison A. Clarke**: Formal analysis, Data Curation, Writing — Review & Editing. **Tara R. Hawkinson**: Formal analysis, Data Curation, Writing — Review & Editing. **Terrymar Medina**: Formal analysis, Data Curation, Writing — Review & Editing. **Ramon C. Sun**: Conceptualization, Methodology, Software, Validation, Formal analysis, Investigation, Resources, Data Curation, Writing — Original Draft, Writing — Review & Editing, Visualization, Supervision. **Todd A. Lydic**: Formal analysis, Investigation, Data Curation, Writing — Original Draft, Writing — Review & Editing. **Terry Hinds Jr.**: Methodology, Software, Validation, Formal analysis, Investigation, Resources, Data Curation, Writing — Original Draft, Writing — Review & Editing, Supervision. **J. Mark Brown**: Data Curation, Methodology, Validation, Formal analysis, Resources, Data Curation, & Funding acquisition. **Samir Softic**: Resources, Writing — Original Draft, Writing — Review & Editing, Supervision, Project administration, Funding acquisition. **Gregory A. Graf**: Conceptualization, Resources, Data Curation, Writing — Original Draft, Writing — Review & Editing, Supervision, Project administration, Funding acquisition. **Robert N. Helsley**: Conceptualization, Data Curation, Methodology, Validation, Formal analysis, Investigation, Resources, Data Curation, Writing — Original Draft, Writing — Review & Editing, Visualization, Supervision, Project administration, Funding acquisition.

FUNDING SOURCES

DECLARATION OF COMPETING INTEREST

The authors declare that they have no known competing financial interests or personal relationships that could have appeared to influence the work reported in this paper.

DATA AVAILABILITY

Data will be made available on request.

ACKNOWLEDGEMENTS

APPENDIX A. SUPPLEMENTARY DATA

Supplementary data to this article can be found online at https://doi.org/10.1016/j.molmet.2023.101815.

REFERENCES

[1] Rinella ME, Lazarus JV, Ratziu V, Francque SM, Sanyal AJ, Kanwal F, et al. A multi-society Delphi consensus statement on new fatty liver disease nomenclature. Hepatology 2023. Online ahead of print. PMID: 37363821.

[2] Badmus OO, Hillhouse SA, Anderson CD, Hinds TD, Stec DE. Molecular mechanisms of metabolic associated fatty liver disease (MAFLD): functional analysis of lipid metabolism pathways. Clin Sci (Lond) 2022;136:1347—66.

[3] Allen AM, Therneau TM, Larson JJ, Coward A, Somers VK, Kamath PS. Nonalcoholic fatty liver disease incidence and impact on metabolic burden and death: a 20 year-community study. Hepatology 2018;67:1726—36.

[4] Calzadilla Bertot L, Adams LA. The natural course of non-alcoholic fatty liver disease. Int J Mol Sci 2016;17.

[5] Burra P, Bizzaro D, Gonta A, Shalaby S, Gambato M, Morelli MC, et al. Clinical impact of sexual dimorphism in non-alcoholic fatty liver disease (NAFLD) and non-alcoholic steatohepatitis (NASH). Liver Int 2021;41:1713—33.

[6] Balakrishnan M, Patel P, Dunn-Valadez S, Dao C, Khan V, Ali H, et al. Women have a lower risk of nonalcoholic fatty liver disease but a higher risk of progression vs men: a systematic Review and meta-analysis. Clin Gastroenterol Hepatol 2021;19:61—71 e15.

[7] Ballestri S, Nascimbeni F, Baldelli E, Marrazzo A, Romagnoli D, Lonardo A. NAFLD as a sexual dimorphic disease: role of gender and reproductive status in the development and progression of nonalcoholic fatty liver disease and inherent cardiovascular risk. Adv Ther 2017;34:1291—326.

[8] Marinou K, Adiels M, Hodson L, Frayn KN, Karpe F, Fielding BA. Young women partition fatty acids towards ketone body production rather than VLDL-TAG synthesis, compared with young men. Br J Nutr 2011;105:857—65.

[9] Lonardo A, Nascimbeni F, Ballestri S, Fairweather D, Win S, Than TA, et al. Sex differences in nonalcoholic fatty liver disease: state of the art and identification of Research gaps. Hepatology 2019;70:1457—69.

[10] Wolfgang MJ, Lane MD. Hypothalamic malonyl-CoA and CPT1c in the treatment of obesity. FEBS J 2011;278:552—8.

[11] Das M, Sha J, Hidalgo B, Aslibekyan S, Do AN, Zhi D, et al. Association of DNA methylation at CPT1A locus with metabolic syndrome in the genetics of lipid lowering drugs and diet network (GOLDN) study. PLoS One 2016;11:e0145789.

[12] Frazier-Wood AC, Aslibekyan S, Absher DM, Hopkins PN, Sha J, Tsai MY, et al. Methylation at CPT1A locus is associated with lipoprotein subfraction profiles. J Lipid Res 2014;55:1324—30.

[13] Lemas DJ, Wiener HW, O'Brien DM, Hopkins S, Stanhope KL, Havel PJ, et al. Genetic polymorphisms in carnitine palmitoyltransferase 1A gene are associated with variation in body composition and fasting lipid traits in Yup'Ik Eskimos. J Lipid Res 2012;53:175—84.

[14] Skotte L, Koch A, Yakimov V, Zhou S, Soborg B, Andersson M, et al. CPT1A missense mutation associated with fatty acid metabolism and reduced height in Greenlanders. Circ Cardiovasc Genet 2017;10.

[15] Schoors S, Bruning U, Missiaen R, Queiroz KC, Borgers G, Elia I, et al. Fatty acid carbon is essential for dNTP synthesis in endothelial cells. Nature 2015;520:192—7.

[16] Helsley RN, Miyata T, Kadam A, Varadharajan V, Sangwan N, Huang EC, et al. Gut microbial trimethylamine is elevated in alcohol-associated hepatitis and contributes to ethanol-induced liver injury in mice. Elife 2022:11.

[17] Helsley RN, Varadharajan V, Brown AL, Gromovsky AD, Schugar RC, Ramachandiran I, et al. Obesity-linked suppression of membrane-bound O-acyltransferase 7 (MBOAT7) drives non-alcoholic fatty liver disease. Elife 2019;8.

[18] Delekta PC, Lydic TA, Hammer ND. Isolation of lipoprotein particles from chicken egg yolk for the study of bacterial pathogen fatty acid incorporation into membrane phospholipids. J Vis Exp 2019;147.

[19] Delekta PC, Shook JC, Lydic TA, Mulks MH, Hammer ND. Staphylococcus aureus utilizes host-derived lipoprotein particles as sources of fatty acids. J Bacteriol 2018;200.

[20] Lydic TA, Busik JV, Reid GE. A monophasic extraction strategy for the simultaneous lipidome analysis of polar and nonpolar retina lipids. J Lipid Res 2014;55:1797—809.

[21] Andersen MK, Hoiem TS, Claes BSR, Balluff B, Martin-Lorenzo M, Richardsen E, et al. Spatial differentiation of metabolism in prostate cancer tissue by MALDI-TOF MSI. Cancer Metabol 2021;9:9.

[22] Creeden JF, Kipp ZA, Xu M, Flight RM, Moseley HNB, Martinez GJ, et al. Hepatic kinome atlas: an in-depth identification of kinase pathways in liver fibrosis of humans and rodents. Hepatology 2022;76:1376—88.

[23] Badmus OO, Kipp ZA, Bates EA, da Silva AA, Taylor LC, Martinez GJ, et al. Loss of hepatic PPARalpha in mice causes hypertension and cardiovascular disease. Am J Physiol Regul Integr Comp Physiol 2023;325:R81—95.

[24] Bates EA, Kipp ZA, Martinez GJ, Badmus OO, Soundarapandian MM, Foster D, et al. Suppressing hepatic UGT1A1 increases plasma bilirubin, lowers plasma urobilin, reorganizes kinase signaling pathways and lipid species and improves fatty liver disease. Biomolecules 2023;13.

[25] Creeden JF, Alganem K, Imami AS, Brunicardi FC, Liu SH, Shukla R, et al. Kinome array profiling of patient-derived pancreatic ductal adenocarcinoma identifies differentially active protein tyrosine kinases. Int J Mol Sci 2020;21.

[26] Appuhamy JA, Nayananjalie WA, England EM, Gerrard DE, Akers RM, Hanigan MD. Effects of AMP-activated protein kinase (AMPK) signaling and essential amino acids on mammalian target of rapamycin (mTOR) signaling and protein synthesis rates in mammary cells. J Dairy Sci 2014;97:419—29.

[27] Dorsett CR, McGuire JL, Niedzielko TL, DePasquale EA, Meller J, Floyd CL, et al. Traumatic brain injury induces alterations in cortical glutamate uptake without a reduction in glutamate transporter-1 protein expression. J Neurotrauma 2017;34:220—34.

[28] McGuire JL, Depasquale EA, Funk AJ, O'Donnovan SM, Hasselfeld K, Marwaha S, et al. Abnormalities of signal transduction networks in chronic schizophrenia. NPJ Schizophr 2017;3:30.

[29] DePasquale EAK, Alganem K, Bentea E, Nawreen N, McGuire JL, Naji F, et al. KRSA: network-based prediction of differential kinase activity from kinome array data. bioRxiv 2020. 2020.2008.2026.268581.

[30] Chirumamilla CS, Fazil M, Perez-Novo C, Rangarajan S, de Wijn R, Ramireddy P, et al. Profiling activity of cellular kinases in migrating T-cells. Methods Mol Biol 2019;1930:99—113.

[31] Franklin MP, Sathyanarayan A, Mashek DG. Acyl-CoA thioesterase 1 (ACOT1) regulates PPARalpha to couple fatty acid flux with oxidative capacity during fasting. Diabetes 2017;66:2112—23.

[32] Mina AI, LeClair RA, LeClair KB, Cohen DE, Lantier L, Banks AS. CalR: a web-based analysis tool for indirect calorimetry experiments. Cell Metabol 2018;28: 656—666.e651.

[33] Geisler CE, Hepler C, Higgins MR, Renquist BJ. Hepatic adaptations to maintain metabolic homeostasis in response to fasting and refeeding in mice. Nutr Metab 2016;13:62.

[34] Sun W, Nie T, Li K, Wu W, Long Q, Feng T, et al. Hepatic CPT1A facilitates liver-adipose cross-talk via induction of FGF21 in mice. Diabetes 2021.

[35] Benjamin B, Wada Y, Grundy SM, Szuszkiewicz-Garcia M, Vega GL. Fatty acid oxidation in normotriglyceridemic men. J Clin Lipidol 2016;10:283—8.

[36] Boden G. Free fatty acids, insulin resistance, and type 2 diabetes mellitus. Proc Assoc Am Phys 1999;111:241—8.

[37] Schooneman MG, Vaz FM, Houten SM, Soeters MR. Acylcarnitines: reflecting or inflicting insulin resistance? Diabetes 2013;62:1—8.

[38] Matthews DR, Hosker JP, Rudenski AS, Naylor BA, Treacher DF, Turner RC. Homeostasis model assessment: insulin resistance and beta-cell function from fasting plasma glucose and insulin concentrations in man. Diabetologia 1985;28:412—9.

[39] Mashek DG, Khan SA, Sathyanarayan A, Ploeger JM, Franklin MP. Hepatic lipid droplet biology: getting to the root of fatty liver. Hepatology 2015;62:964—7.

[40] Seebacher F, Zeigerer A, Kory N, Krahmer N. Hepatic lipid droplet homeostasis and fatty liver disease. Semin Cell Dev Biol 2020;108:72—81.

[41] Helsley RN, Park SH, Vekaria HJ, Sullivan PG, Conroy LR, Sun RC, et al. Keto-hexokinase-C regulates global protein acetylation to decrease carnitine palmitoyltransferase 1a-mediated fatty acid oxidation. J Hepatol 2023;79:25—42.

[42] Hall Z, Bond NJ, Ashmore T, Sanders F, Ament Z, Wang X, et al. Lipid zonation and phospholipid remodeling in nonalcoholic fatty liver disease. Hepatology 2017;65:1165—80.

[43] Hijmans BS, Grefhorst A, Oosterveer MH, Groen AK. Zonation of glucose and fatty acid metabolism in the liver: mechanism and metabolic consequences. Biochimie 2014;96:121—9.

[44] Krahmer N, Guo Y, Wilfling F, Hilger M, Lingrell S, Heger K, et al. Phosphatidylcholine synthesis for lipid droplet expansion is mediated by localized activation of CTP:phosphocholine cytidylyltransferase. Cell Metabol 2011;14:504—15.

[45] Tauchi-Sato K, Ozeki S, Houjou T, Taguchi R, Fujimoto T. The surface of lipid droplets is a phospholipid monolayer with a unique Fatty Acid composition. J Biol Chem 2002;277:44507—12.

[46] Li Z, Agellon LB, Allen TM, Umeda M, Jewell L, Mason A, et al. The ratio of phosphatidylcholine to phosphatidylethanolamine influences membrane integrity and steatohepatitis. Cell Metabol 2006;3:321—31.

[47] Zhao Y, Su B, Jacobs RL, Kennedy B, Francis GA, Waddington E, et al. Lack of phosphatidylethanolamine N-methyltransferase alters plasma VLDL phospholipids and attenuates atherosclerosis in mice. Arterioscler Thromb Vasc Biol 2009;29:1349—55.

[48] Seubnooch P, Montani M, Tsouka S, Claude E, Rafiqi U, Perren A, et al. Characterisation of hepatic lipid signature distributed across the liver zonation using mass spectrometry imaging. JHEP Rep 2023;5:100725.

[49] Zhang H, Pan YZ, Cheung M, Cao M, Yu C, Chen L, et al. LAMB3 mediates apoptotic, proliferative, invasive, and metastatic behaviors in pancreatic cancer by regulating the PI3K/Akt signaling pathway. Cell Death Dis 2019;10:230.

[50] Gao G, Chen FJ, Zhou L, Su L, Xu D, Xu L, et al. Control of lipid droplet fusion and growth by CIDE family proteins. Biochim Biophys Acta Mol Cell Biol Lipids 2017;1862:1197—204.

[51] Kuch EM, Vellaramkalayil R, Zhang I, Lehnen D, Brugger B, Sreemmel W, et al. Differentially localized acyl-CoA synthetase 4 isoenzymes mediate the metabolic channeling of fatty acids towards phosphatidylinositol. Biochim Biophys Acta 2014;1841:227—39.

[52] Hishikawa D, Yanagida K, Nagata K, Kanatani A, Iizuka Y, Hamano F, et al. Hepatic levels of DHA-containing phospholipids instruct SREBP1-mediated synthesis and systemic delivery of polyunsaturated fatty acids. iScience 2020;23:101495.

[53] Hashidate-Yoshida T, Harayama T, Hishikawa D, Morimoto R, Hamano F, Tokuoka SM, et al. Fatty acid remodeling by LPCAT3 enriches arachidonate in phospholipid membranes and regulates triglyceride transport. Elife 2015;4.

[54] Petkevicius K, Palmgren H, Glover MS, Ahnmark A, Andreasson AC, Madeyski-Bengtson K, et al. TLCD1 and TLCD2 regulate cellular phosphatidylethanolamine composition and promote the progression of non-alcoholic steatohepatitis. Nat Commun 2022;13:6020.

[55] de la Rosa Rodriguez MA, Kersten S. Regulation of lipid droplet-associated proteins by peroxisome proliferator-activated receptors. Biochim Biophys Acta Mol Cell Biol Lipids 2017;1862:1212—20.

[56] Langhi C, Baldan A. CIDEC/FSP27 is regulated by peroxisome proliferator-activated receptor alpha and plays a critical role in fasting- and diet-induced hepatosteatosis. Hepatology 2015;61:1227—38.

[57] Zandbergen F, Mandard S, Escher P, Tan NS, Patsouris D, Jatkoe T, et al. The G0/G1 switch gene 2 is a novel PPAR target gene. Biochem J 2005;392: 313—24.

[58] Yang X, Lu X, Lombes M, Rha GB, Chi YI, Guerin TM, et al. The G(0)/G(1) switch gene 2 regulates adipose lipolysis through association with adipose triglyceride lipase. Cell Metabol 2010;11:194—205.

[59] Grist M, Wambolt RB, Bondy GP, English DR, Allard MF. Estrogen replacement stimulates fatty acid oxidation and impairs post-ischemic recovery of hearts from ovariectomized female rats. Can J Physiol Pharmacol 2002;80:1001—7.

[60] Gao H, Falt S, Sandelin A, Gustafsson JA, Dahlman-Wright K. Genome-wide identification of estrogen receptor alpha-binding sites in mouse liver. Mol Endocrinol 2008;22:10—22.

[61] DeLong CJ, Shen YJ, Thomas MJ, Cui Z. Molecular distinction of phosphatidylcholine synthesis between the CDP-choline pathway and phosphatidylethanolamine methylation pathway. J Biol Chem 1999;274:29683—8.

[62] Reo NV, Adinehzadeh M, Foy BD. Kinetic analyses of liver phosphatidylcholine and phosphatidylethanolamine biosynthesis using (13)C NMR spectroscopy. Biochim Biophys Acta 2002;1580:171—88.

[63] Ridgway ND, Vance DE. Specificity of rat hepatic phosphatidylethanolamine N-methyltransferase for molecular species of diacyl phosphatidylethanolamine. J Biol Chem 1988;263:16856—63.

[64] Watkins SM, Zhu X, Zeisel SH. Phosphatidylethanolamine-N-methyltransferase activity and dietary choline regulate liver-plasma lipid flux and essential fatty acid metabolism in mice. J Nutr 2003;133:3386—91.

[65] Jacobs RL, Zhao Y, Koonen DP, Sletten T, Su B, Lingrell S, et al. Impaired de novo choline synthesis explains why phosphatidylethanolamine N-methyltransferase-deficient mice are protected from diet-induced obesity. J Biol Chem 2010;285:22403—13.

[66] Wan S, van der Veen JN, Bakala N'Goma JC, Nelson RC, Vance DE, Jacobs RL. Hepatic PEMT activity mediates liver health, weight gain, and insulin resistance. Faseb J 2019;33:10986—95.

[67] Zhu X, Song J, Mar MH, Edwards LJ, Zeisel SH. Phosphatidylethanolamine N-methyltransferase (PEMT) knockout mice have hepatic steatosis and abnormal hepatic choline metabolite concentrations despite ingesting a recommended dietary intake of choline. Biochem J 2003;370:987—93.

[68] Bale G, Vishnubhotla RV, Mitnala S, Sharma M, Padaki RN, Pawar SC, et al. Whole-exome sequencing identifies a variant in phosphatidylethanolamine N-methyltransferase gene to be associated with lean-nonalcoholic fatty liver disease. J Clin Exp Hepatol 2019;9:561—8.

[69] Song J, da Costa KA, Fischer LM, Kohlmeier M, Kwock L, Wang S, et al. Polymorphism of the PEMT gene and susceptibility to nonalcoholic fatty liver disease (NAFLD). Faseb J 2005;19:1266—71.

[70] Resseguie M, Song J, Niculescu MD, da Costa KA, Randall TA, Zeisel SH. Phosphatidylethanolamine N-methyltransferase (PEMT) gene expression is induced by estrogen in human and mouse primary hepatocytes. Faseb J 2007;21:2622—32.

[71] Saigo Y, Sasase T, Uno K, Shinozaki Y, Maekawa T, Sano R, et al. Establishment of a new nonalcoholic steatohepatitis model; Ovariectomy exacerbates nonalcoholic steatohepatitis-like pathology in diabetic rats. J Pharmacol Toxicol Methods 2022;116:107190.

[72] Leonard AE, Kelder B, Bobik EG, Chuang LT, Lewis CJ, Kopchick JJ, et al. Identification and expression of mammalian long-chain PUFA elongation enzymes. Lipids 2002;37:733—40.

[73] Moon YA, Hammer RE, Horton JD. Deletion of ELOVL5 leads to fatty liver through activation of SREBP-1c in mice. J Lipid Res 2009;50:412—23.

[74] Sekiya M, Yahagi N, Matsuzaka T, Najima Y, Nakakuki M, Nagai R, et al. Polyunsaturated fatty acids ameliorate hepatic steatosis in obese mice by SREBP-1 suppression. Hepatology 2003;38:1529—39.

[75] DeBose-Boyd RA, Ye J. SREBPs in lipid metabolism, insulin signaling, and beyond. Trends Biochem Sci 2018;43:358—68.

[76] Wicks SE, Vandanmagsar B, Haynie KR, Fuller SE, Warfel JD, Stephens JM, et al. Impaired mitochondrial fat oxidation induces adaptive remodeling of muscle metabolism. Proc Natl Acad Sci U S A 2015;112:E3300—9.

[77] Papsdorf K, Miklas JW, Hosseini A, Cabruja M, Morrow CS, Savini M, et al. Lipid droplets and peroxisomes are co-regulated to drive lifespan extension in response to mono-unsaturated fatty acids. Nat Cell Biol 2023;25:672—84.

[78] Wang Y, Li C, Zhang J, Xu X, Fu L, Xu J, et al. Polyunsaturated fatty acids promote the rapid fusion of lipid droplets in Caenorhabditis elegans. J Biol Chem 2022;298:102179.

[79] Matsusue K, Kusakabe T, Noguchi T, Takiguchi S, Suzuki T, Yamano S, et al. Hepatic steatosis in leptin-deficient mice is promoted by the PPARgamma target gene Fsp27. Cell Metabol 2008;7:302—11.

[80] Lee SM, Pusec CM, Norris GH, De Jesus A, Diaz-Ruiz A, Muratalla J, et al. Hepatocyte-specific loss of PPARgamma protects mice from NASH and increases the therapeutic effects of rosiglitazone in the liver. Cell Mol Gastroenterol Hepatol 2021;11:1291—311.

[81] Yu S, Matsusue K, Kashireddy P, Cao WQ, Yeldandi V, Yeldandi AV, et al. Adipocyte-specific gene expression and adipogenic steatosis in the mouse liver due to peroxisome proliferator-activated receptor gamma1 (PPAR-gamma1) overexpression. J Biol Chem 2003;278:498—505.

[82] Fromenty B, Pessayre D. Impaired mitochondrial function in microvesicular steatosis. Effects of drugs, ethanol, hormones and cytokines. J Hepatol 1997;26(Suppl 2):43—53.

[83] Keenan SN, De Nardo W, Lou J, Schittenhelm RB, Montgomery MK, Granneman JG, et al. Perilipin 5 S155 phosphorylation by PKA is required for the control of hepatic lipid metabolism and glycemic control. J Lipid Res 2021;62:100016.

[84] Schott MB, Rasineni K, Weller SG, Schulze RJ, Sletten AC, Casey CA, et al. beta-Adrenergic induction of lipolysis in hepatocytes is inhibited by ethanol exposure. J Biol Chem 2017;292:11815—28.

[85] Yang J, Zhang X, Yi L, Yang L, Wang WE, Zeng C, et al. Hepatic PKA inhibition accelerates the lipid accumulation in liver. Nutr Metab 2019;16:69.